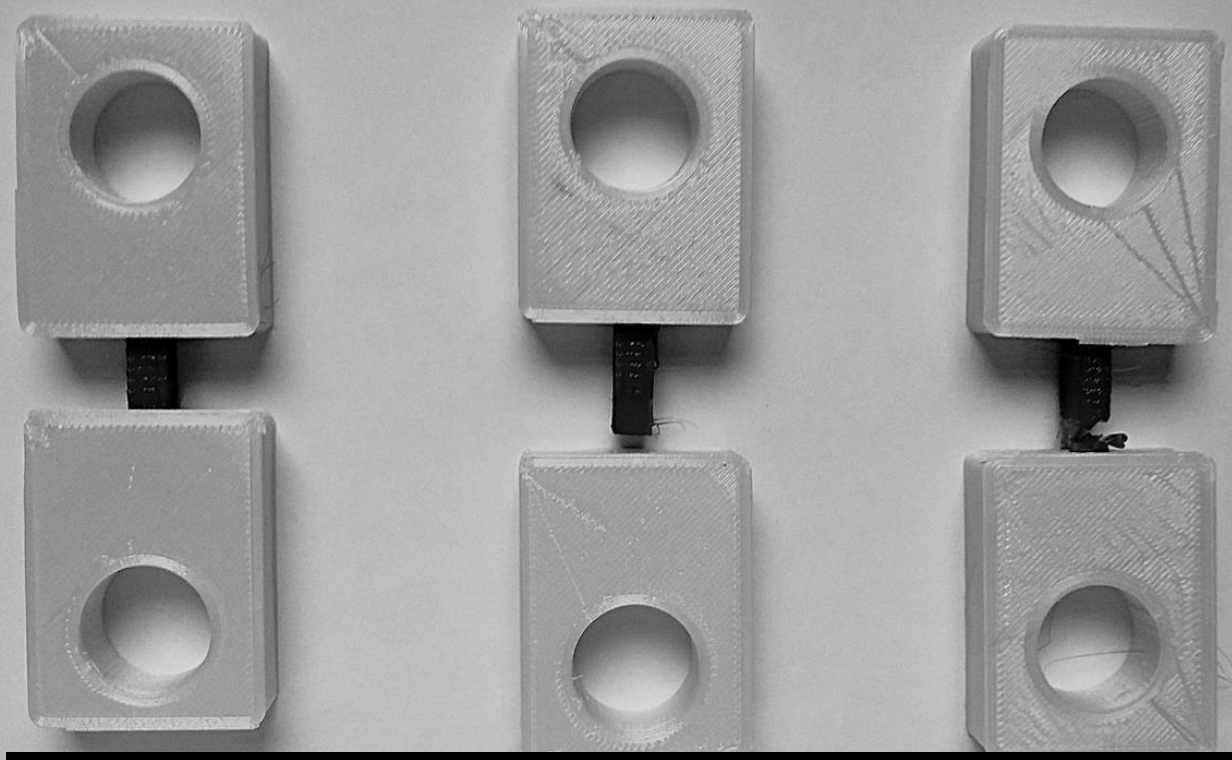

Strength and Fatigue Analysis of FDM-fabricated Non-assembly Bi-material Compliant Mechanisms

Adinda Bunga Juwita

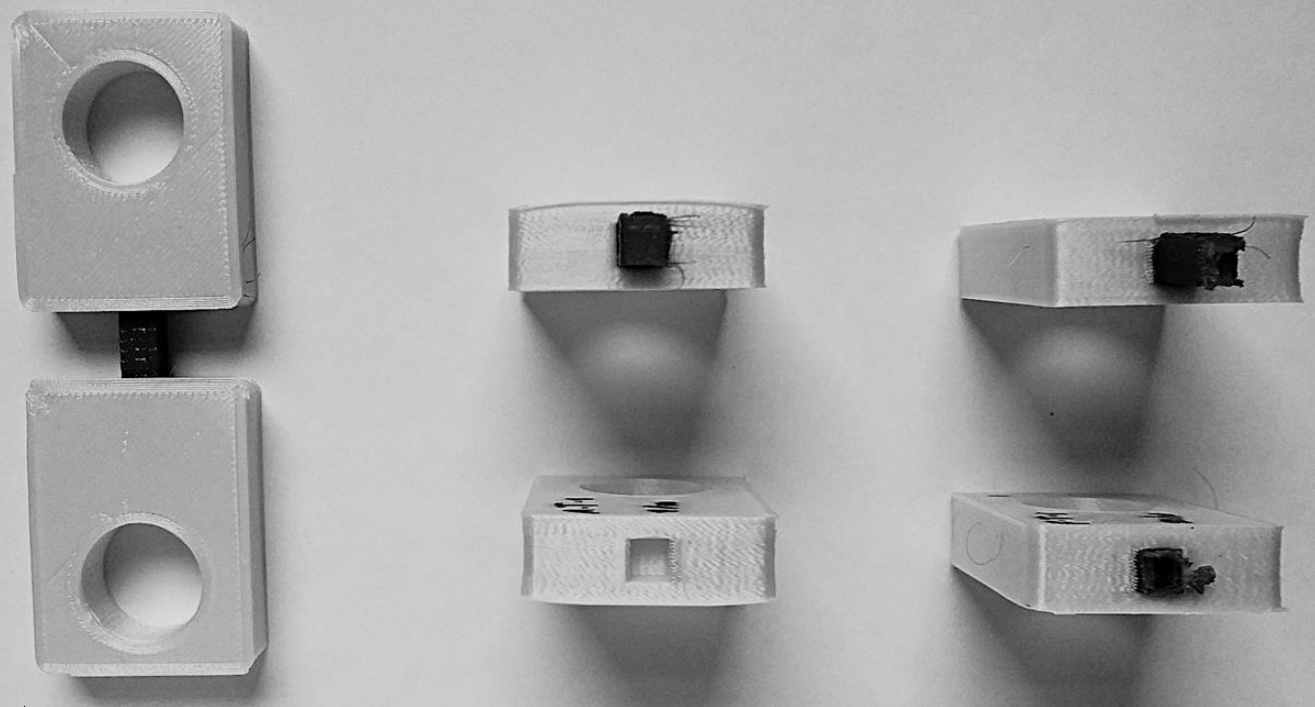

TU Delft

Strength and Fatigue Analysis of FDM-fabricated Non-assembly Bi-material Compliant Mechanisms

By

Adinda Bunga Juwita

in partial fulfilment of the requirements for the degree of

Master of Science
in Biomedical Engineering

at the Delft University of Technology,
to be defended publicly on Thursday, June 20th, 2019 at 1:00 PM.

Supervisor: Prof. Dr. Ir. A.A. Zadpoor
Dr. Ir. G. Smit
J.S. Cuellar, MSc

TU Delft

Preface

Finishing this thesis is not merely fulfilling the requirement to graduate. During my internship period in Indonesia, I observed that the limb prosthesis is still considered a luxury item for many amputees. When I discussed it with the limb prosthesis users, they acknowledged it and felt thankful for their privilege to afford the prosthesis. I could not help but to think of how the low-cost prosthesis project could benefit many people in the future, who never have any idea that they could access it. This experience increased my gratitude that I could take a very small part of the initiation to develop low-cost alternatives to the current prosthetic technology by evaluating the strength and fatigue of parts fabricated with the additive manufacturing process. The journey of learning new subjects was challenging, but I put so much hope that what I did might be useful for others at some point. In addition, this is my way to thank Indonesia Endowment Fund for Education, Ministry of Finance, the Republic of Indonesia for providing full scholarship during the first two years of my master's program.

I experienced many downs throughout the process, but some people who live in this earth ganged up against the negativity and showed their kindness to me. With their help, I was up. I am beyond grateful to have them accompanied this adventure. I would like to thank my daily supervisor, Juan Cuellar, who helped me since the very first day of deciding the topic. His perseverance and knowledge in 3D-printing have inspired me to go down the rabbit hole which leads me to discover the 3D-printing wonderland. Thanks to Gerwin Smit, my supervisor who provided guidance and support, not only for the graduation process but also for the internship. I could not thank him enough for all his kind acts, but I wish he knows that I truly appreciate having him as my supervisor. I would also like to thank my supervisor, Amir Zadpoor, for providing direction, especially in the early and final stages of the project. Thanks to Sander Leeflang for his expertise that helped me during the experiment, Mohammad Mirzaali Mazandarani for facilitating me to access the Abaqus software, and Lourdes Gallastegui Pujana for her advice regarding academic, administrative, and financial matters. Thank you to Niko Eka Putra and Andika Praditya Hadiputra, with whom I shared many hopes and concerns during the master's program. As well, thank you to the members of "Anna's Uncles and Mother" group, who frequently provide many (un)ethical life hacks and have no mercy in making fun of each other. If a laugh box exists, I might not be able to laugh for the rest of my life after overusing it with all of you.

Finally, I dedicate this work to my family. I feel blessed to have Mursid Widanu Kusumo and Ida Zuhida as my parents, Irawati as my mother-in-law, and Tayana Nuraida and Muhammad Johan Adhibuana as my siblings. Thank you for your support and encouragement. To my husband, Angku Rai, June was never my favorite month until three years ago when we proposed to each other and a year later our daughter, Warna Senja, arrived. Thank you for ensuring me since then that there is always joy in every act of committing and compromising. Love is overrated but you are the only one who can make me voluntarily accepting my defeat in every boardgame we play.

Adinda Bunga Juwita

Bandung, June 2019

Contents

Abstract

Multi-material compliant mechanisms have shown the potential to be utilized in the upper-limb prosthesis. The mechanisms consist of flexural and rigid parts, where the flexural components can serve as flexible joints between rigid bodies in the device (e.g., finger and finger segments). This configuration is feasible to be fabricated using a type of additive manufacturing called Fused Deposition Modelling (FDM) process, without the need of further assembly and extensive post-processing. Knowledge of the mechanical characteristics of such mechanisms, however, is still limited. Therefore, this study presents the strength and fatigue characteristics of bi-material compliant mechanisms to determine the feasibility of applying the mechanisms in the upper-limb prosthesis for long-term use. The basis of the mechanisms was a configuration of two rigid clamps and a flexible beam that were automatically assembled during manufacturing. Two materials selections (PLA-TPU and Tough PLA-TPU) and three geometries (rectangular, cylindrical, and tapered-shaped interface) were used to create six groups of samples. These groups were subjected to tensile testing and fatigue testing to assess their strength and fatigue behavior. The results of mechanical testing were also verified with the results of finite element simulation. It was found that four groups fulfilled the strength requirement, which were mechanisms in both material configurations with cylindrical and tapered-shaped interface. These groups, however, failed to demonstrate their durability during fatigue testing. Finally, the proposed method of fabrication and mechanical testing as well as the obtained mechanical characteristics of the mechanisms were analyzed to give insights for future development.

I. Introduction

1.1 Non-assembly multi-material compliant mechanisms

Multi-material compliant mechanisms with the configuration of flexible and rigid parts show the promising application in the upper-limb prosthesis. The flexural components fabricated from a material with relatively low elastic moduli have the potential to serve as joints between rigid bodies in the device (e.g. finger segments) made from a material with higher elastic moduli [1]. The mechanisms offer several advantages. The rigid parts with high yield strength are beneficial to prevent mechanical failure such as breaking, thus enhancing the life-span of the upper-limb prosthesis. The flexible components, on the other hand, have high compliance which is useful to transfer motion by using deflection. In comparison with conventional rigid links and joints, compliant mechanisms usually have hinge-less designs with fewer movable joints. These designs of compliant mechanisms can reduce wear and backlash; problems that often occur in the conventional rigid links and joints [2, 3]. In addition, compliant mechanisms offer ease of assembly with simple steps, if at all, or no further assembly needed when using suitable designs and fabrication methods [2, 4].

Multi-material molding and additive manufacturing are two common methods to fabricate multi-material compliant mechanisms [5]. In multi-material molding, several types of polymers form compliant mechanisms after changing the state from liquid to solid through physical or chemical reactions inside the mold. This method is suitable for producing similar compliant mechanisms in large quantity [5, 6]. For low-volume manufacturing that also needs customization, the second method, additive manufacturing, is more practical [5, 6]. By accumulating materials layer by layer, additive manufacturing (AM) process can construct a 3D object with optimized geometries with desired material distributions [7]. Using the correct settings in AM enables various customization that is beneficial to achieve the desired end-product without further assembly or extensive post-processing [7, 8]. Therefore, this process is convenient for fabricating multi-material compliant mechanisms in the upper-limb prosthesis with specific characteristics that meet the user needs.

The development of an AM process called Fused Deposition Modelling (FDM) contributes to the ease of fabrication of non-assembly multi-material compliant mechanisms. In this process, the machine has at least one nozzle to extrude semi-solid material by applying specific pressure to deposit a layer [7]. In case of having only one nozzle, there are various bonding methods such as welding or adhesive joining to form multi-material mechanisms from several fabricated parts. However, the process is time-consuming, and the strength of the bonded parts is lower than each of the original part [9]. Using FDM machine that has at least two nozzles can eliminate the need for additional bonding and assembly methods after fabrication. With two nozzles, the machine can extrude two different materials. The extruded filament from one material attaches with the adjacent, previously deposited filaments from similar or different materials. The strength of the end part depends on the bond strength of each filament [10, 11]. Hence, not only the geometry of the mechanisms but also the combination of materials used need to be considered to produce compliant mechanisms with high strength.

1.2 Problem definition

The mechanical characteristics of certain mechanisms need to be taken into account to validate the functionality and durability in a specific application. Several studies have been conducted to understand the mechanical properties of additively manufactured part fabricated with a particular material. The strength of multi-material mechanisms from components that are attached using various bonding methods after fabrication has also been addressed. However, currently, there is limited knowledge of the mechanical properties of additively manufactured multi-material mechanisms which consist of flexible and rigid components that are fabricated in a single step. Such information is essential to determine the feasibility of applying the mechanisms in the upper-limb prosthesis.

1.3 Objective

The objective of this study was to analyze the mechanical characteristics of non-assembly bi-material compliant mechanisms, fabricated with FDM method. Evaluation of the experimental testing results was made to determine the feasibility of applying the mechanisms with specific materials, geometries, and fabrication method in the upper-limb prosthesis that can be used for long term.

II. Methods

2.1 Design considerations

The design considerations of the non-assembly multi-material compliant mechanisms are presented in this section. In this study, the considerations were derived from the objective that the mechanisms need to be suitable for the upper-limb prosthesis and fabricated using an additive manufacturing process.

2.1.1 Strength and fatigue characteristics

The strength and fatigue of the non-assembly compliant mechanisms hold critical importance as they determine the functionality and durability of the mechanisms. The mechanisms can mechanically fail under different circumstances. The mechanisms can break if they are subjected to a higher load than the ultimate tensile strength, also known as the tensile failure [12]. However, even load that is smaller than the yield stress can also be responsible for fracture after several amounts of loading and unloading. This fatigue failure happens when the repetitive loads initiate microdamage in the mechanisms [13]. The small cracks within the mechanisms can build up and lead to mechanical failure [12, 13].

The strength and fatigue requirements of the mechanisms were based on several assumptions. First, the mechanisms are used as flexural joints in each hand digit of the upper-limb prosthesis. Second, the mechanisms can imitate the strength of the human hand. Lastly, the mechanisms can last for a year of regular use.

In terms of strength, the human hand can exert up to 400 N when performing grasp with all hand digits. The functional grasping force of the average human hand, however, falls in the range between 0 to 67 N [14]. Therefore, the mechanisms need to withstand the load of at least 67 N.

Fatigue failure of the mechanisms needs to be avoided to prolong the life of the device. It is estimated that an upper-limb prosthesis can reach 100,000 cycles of opening-closing annually to support the user for performing daily activities [15]. Therefore, using the same number of cycles, the mechanisms need to endure fatigue testing with repetitive loads that are alternating below the yield strength.

2.1.2 Geometry of the mechanisms

After determining the strength and fatigue limit, the next consideration is the geometry of the mechanisms. The selected geometry can affect not only the mechanical behavior of the mechanisms but also the ease of fabrication and the ease to conduct the mechanical evaluation of the mechanisms.

As compliant mechanisms are characterized by the ability of the mechanisms to use elastic deformation for transferring motion and force [2, 3], having at least one flexural component in the mechanisms is essential. The suitable geometry is needed to produce a compliant part with high-strength. Nevertheless, it is important to recognize that the geometry itself is not the only factor which affects the strength and compliance in the mechanisms. Other parameters, such as the mechanical properties of the material, also contribute to the mechanical behavior of the mechanisms [2].

There was a necessity to restrict the shape and size of the mechanisms in this study as there is a limitation in the size of upper-limb prosthesis. This replacement limb device usually designed using dimensions that match with the normal hand to meet the user requirement to use a device with a high resemblance to the appearance of the actual hand [16]. **Table 1** shows the reference values of the size of the human index finger [17]. Calculation of the length of each finger segment was done using the ratio of the length of the finger segment and the length of the entire finger [18]. The results of the calculation can be seen in **Table 2** [17, 18]. The size constraints were decided based on these values. The width of the compliant mechanisms must not exceed the fingerbreadth while the length of the mechanisms must not higher than the length of the shortest finger segment (i.e., fingertip to distal phalanx). Fabricating the mechanisms with these geometry restrictions is also feasible using the available additive manufacturing process. Lastly, the mechanisms also need to have the appropriate size and shape which fit the testing machine for mechanical evaluation.

2.1.3 Manufacturing process and materials

Regarding the manufacturing process, the designs shall be suitable to be produced using available additive manufacturing technique with no further assembly required. Relatively short printing time and minimum post-processing are also desirable. The range of materials that can be chosen also depends on the selected manufacturing process. Therefore, it is necessary to evaluate whether the designed mechanisms can achieve the expected strength and fatigue characteristics using the available materials that are compatible with current additive manufacturing technology.

2.2 Design of non-assembly multi-material compliant mechanisms

As can be seen in **Figure 2**, the mechanisms consisted of two rigid clamps and a flexible beam with the interface section between the beam and the clamps. There were three different configurations of the mechanisms, which were based on the shape of the interface: rectangular (**Figure 3.A**), cylindrical (**Figure 3.B**), and tapered-shaped interface (**Figure 3.C**). Rectangular shape was used to evaluate whether the simplest configuration could work for upper-limb prosthesis. Cylindrical shape, with the higher surface area than the rectangular interface, was chosen to investigate the effect of increasing surface area of the interface between rigid bodies and a compliant beam to the strength of the mechanisms. Tapered-shape interface was selected to reduce the stress concentration, as a straight beam in the mechanisms had discontinuities which increased the stress concentration [19]. The technical drawings of the mechanisms can be found in **Appendix A**.

Table 1. Index finger size [17]

Parameter	Female	Male	Mixed
Length (mm)	70 ± 4	78 ± 5	74 ± 6
Fingerbreadth (mm)	15 ± 1	19 ± 1	17 ± 2

Despite having differences in the shape of the interface, the rest of the mechanisms had the same shape and size. In every configuration, the flexible beam was 10 mm long, and the total length of the mechanisms was 90 mm. The total length value was selected to fit the fixtures in

the testing machine. Each clamp had a hole that also matched the diameter of fixtures in a testing machine. The flexible beam, as well as the interface, had a thickness of 0.4 mm in all configurations. This value was selected since the smallest thickness of compliant mechanisms for additively manufactured upper-limb prosthesis found in literature was 0.4 mm [20]. However, the thickness was changed to 5 mm since the results from tensile testing showed that the yield strength of the 0.4 mm beam produced the value of minimum stress for fatigue testing in the range of measurement error of the test system.

Table 2. Length of index finger segments [17, 18]

Finger segment*	**Percentage of the finger segment length to the entire index finger [18]**	**Length of index finger segment in mm (mixed population) [17, 18]**
Fingertip to distal phalanx	27.80	20.57
Medial phalanx	30.97	22.92
Proximal phalanx, including the web of proximal phalanx	41.23	30.51

***(see **Figure 1** for the illustration of finger segments)

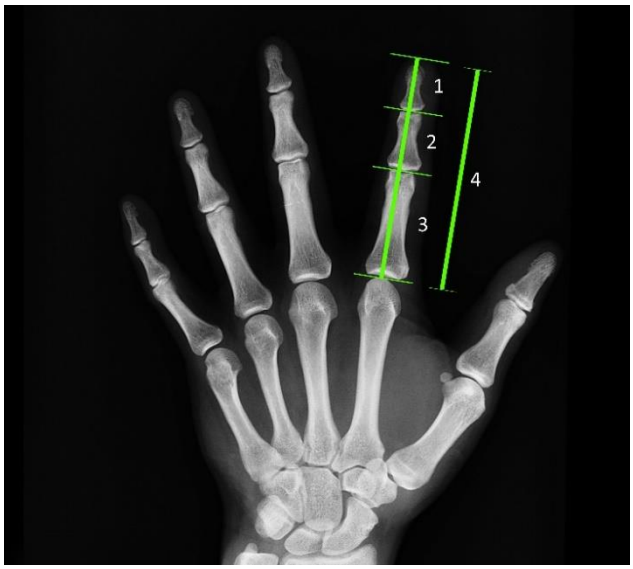

Figure 1. Segments of index finger. 1. Fingertip to distal phalanx. 2. Medial phalanx. 3. Proximal phalanx, including the web of proximal phalanx. 4. The whole length of index finger. Adapted from [18] using the stock image.

2.3 Fabrication method

Additive manufacturing covers various fabrication methods that deposit materials in a relatively thin layer by using certain machine architecture and physical transformation of material. Selection of fabrication method affects the choice of material and other process parameters, as well as the accuracy of the final part [7].

Fused Deposition Modeling (FDM), a process belongs to the material extrusion method in AM classification, offers a wide range of machines from low-cost to more expensive device that varied in parameter settings. Some of the machines support multi-material fabrication which is due to having more than one nozzle. Polymers that are compatible for FDM are commercially available with competitive cost. However, despite these advantages, FDM also presents several disadvantages such as the anisotropic nature of the final part, the complexity of removing the support structure, and limitations in the size of the fabricated part [7, 21].

The advantages of FDM process increase the accessibility of FDM to individuals. This process becomes a popular method to fabricate open-source upper-limb prosthesis that can be customized to fit the users. Therefore, in this study, FDM was also used as a fabrication method. The aforementioned designs of multi-material compliant mechanisms were imported into the machine code by using Ultimaker Cura software (ultimaker.com) and printed using Ultimaker 3 (ultimaker.com) with dual extrusion.

2.4 Materials

Choosing the materials is a non-trivial matter, especially for flexural part since it provides compliance in the mechanisms. This component can be produced with high elastic moduli material such as aluminum, titanium, and stainless steel [22]. However, not all additive manufacturing technique can process these metals [7]. Furthermore, using these materials leads to the need of manipulating geometry of the mechanisms to produce mechanisms with high-compliance [22]. Therefore, in this study, the selection of materials was constricted to polymers that are widely available for additive manufacturing. Using two different polymers also contributes to constructing compliant mechanisms without extensive geometry manipulation. Polymers with relatively low elastic moduli can be used to fabricate a simple, flexible beam that connects rigid bodies made from polymers with higher elastic moduli.

The combination of Polylactic Acid (PLA) and Thermoplastic Polyurethane (TPU) is frequently used to fabricate upper-limb prosthesis with FDM process. These devices usually consist of rigid finger segments made from PLA that are connected with flexural joints manufactured with TPU that has higher compliance [1, 23-26]. In this study, PLA and TPU 95A filaments from Ultimaker (ultimaker.com) were selected as materials for bi-material compliant mechanisms to identify whether this frequently used combination is actually suitable to create the upper-limb prosthesis for long-term use.

Other than PLA-TPU 95A combination, this study also evaluated the strength and fatigue behavior of Tough PLA-TPU 95A combination. Tough PLA from Ultimaker (ultimaker.com) was selected because the filaments have the similar default printing settings with PLA. The same settings can eliminate the effect that might come from using different printing parameters such as printing speed and temperature. Therefore, only differences in mechanical properties that need to be taken into account. **Table 3** shows the mechanical properties of each material used in this study [27-29]. These data, however, are based on the results of mechanical testing of the specimen that was printed using specific printing settings which had differences with the printing parameters used in this study.

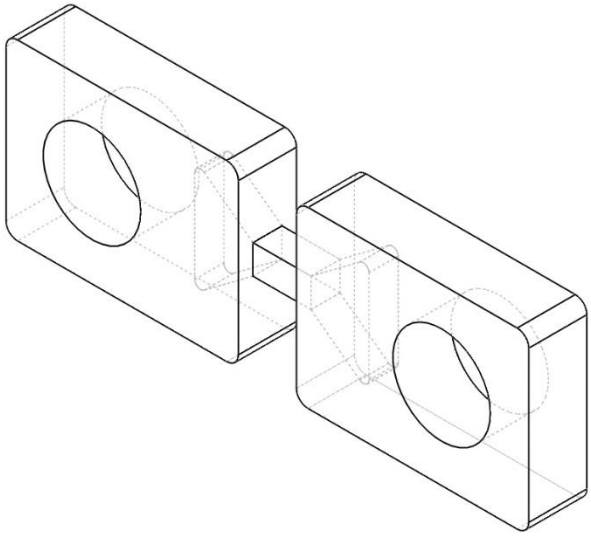

A

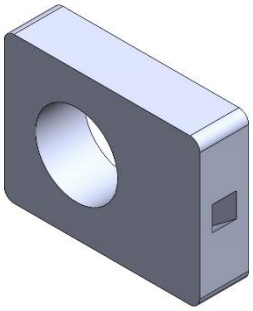

B

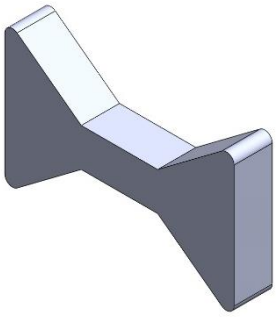

C

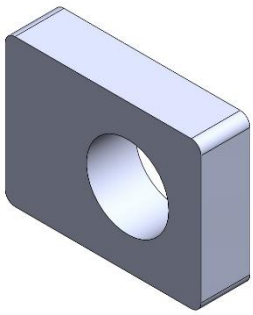

D

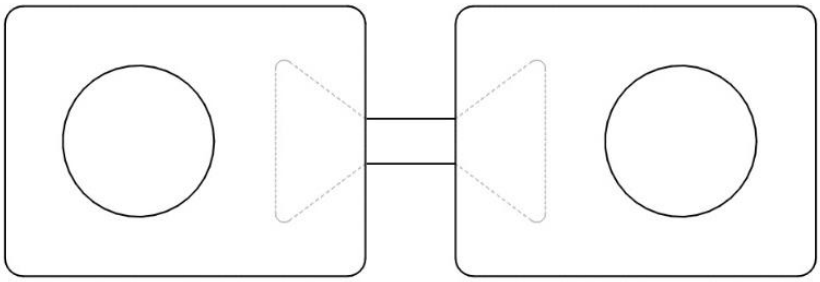

E

Figure 2. Design of bi-material compliant mechanisms. A. Isometric view of the whole part. B. First clamp. C. A flexible beam with the interface section. D. Second clamp. E. Front view of the mechanism. The dash indicates the interface section inside the clamp. Pictures are not in scale.

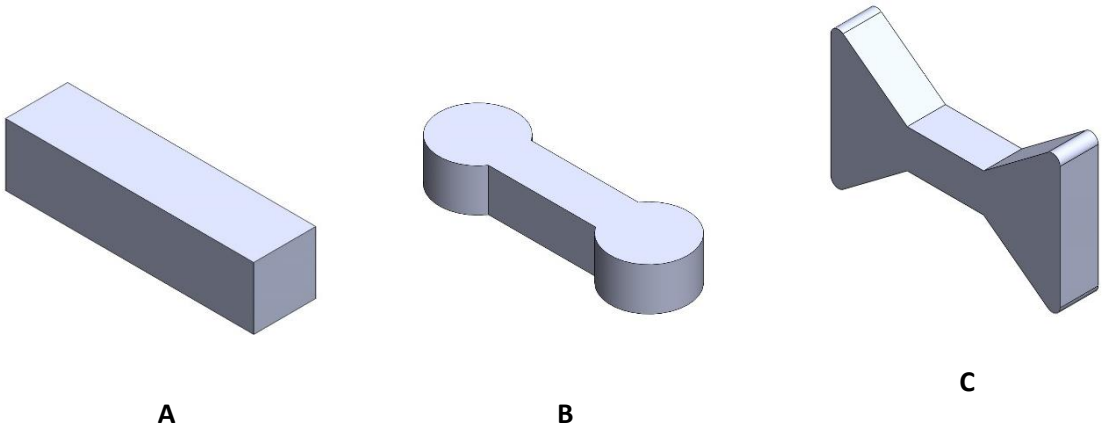

Figure 3. A compliant beam with the rectangular (A), cylindrical (B), and tapered-shaped interface (C)

Table 3. Mechanical properties of Ultimaker polymers [27-29]

Material	Young's Modulus (MPa)	Yield Strength (MPa)	Breaking Strength (MPa)	Yield Strain (%)	Breaking strain (%)
TPU 95A	26	8.6	39	55	580
PLA	2,346.5	49.5	45.6	3.3	5.2
Tough PLA	1,820	37	37	3.1	3.1

The values of load and deformation of the compliant beam at yield point and breaking point were calculated using the normal stress and strain formula with the following equations:

$$F = \sigma . A$$

$$\delta = \epsilon L$$

where F is the maximum load acting over the cross section of the beam at yield or breaking point, σ is the yield stress, A is the cross-sectional area of the beam, δ is the deformation of the beam at yield point, ϵ is the yield strain, and L is the initial length of the beam. In this method, several assumptions were made. The mechanisms were assumed to be homogeneous, isotropic, and linear elastic, which lead to uniform deformation in a cross-section [12]. The effect of differences in printing parameters such as printing speed, nozzle temperature, build plate temperature, and infill density was ignored, as it was impossible to isolate each variable in this study. As PLA and Tough PLA have higher values of elastic modulus and yield strength than TPU 95A, [27-29] it was expected that failure of the compliant beam would occur first. **Table 4** shows the estimated values of load and deformation at yield point of the compliant beam.

Table 4. Estimated values of load and deformation of the compliant beam

Type of compliant beam	Length (mm)	Cross-section area (mm^2)	Yield point	
			Load (N)	Deformation (mm)
0.4 mm thickness	10	2	17.2	5.5
5 mm thickness	10	25	215	5.5

2.5 FDM printing parameters

The bi-material compliant mechanisms were printed using dual extrusion system with the following settings. The diameter of both nozzles was 0.4 mm. The first nozzle extruded PLA or Tough PLA while another nozzle extruded TPU 95A. Default values of printing parameters were used for printing the mechanisms, except for several parameters such as support and build plate adhesion. The printing settings that are listed in **Appendix B** were optimized to fabricate the mechanisms effectively. The mechanisms can be manufactured in a single step using these settings. Each sample required less than two hours of printing time. Manufacturing several samples in one batch, as illustrated in **Figure 4**, can reduce the total printing time in comparison with fabricating one by one. In addition, the process does not need extensive post-processing. The post-processing only consists of separating support material from the flexible beam, which does not require much time.

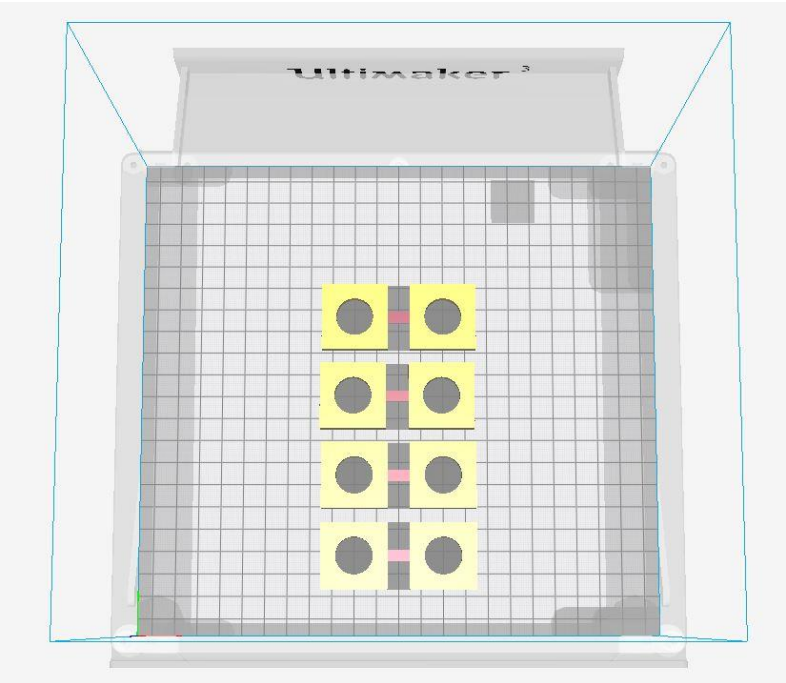

Figure 4. An example of manufacturing four samples in one printing batch

2.6 Mechanical evaluation

Tensile testing and fatigue testing were performed to investigate the strength of the bi-material compliant mechanisms and their behavior under cyclic loading. These mechanisms are classified into six groups according to the materials and the interface shape, as described in **Table 5**.

In tensile testing, Instron ElectroPuls^{TM} E10000 Test System was used to apply axial loading to each sample. The test system applied a force to the clamped specimen by separating the crossheads of the machine. Data from the tests were used to determine yield strength and stiffness value of each sample. The configuration of the test system can be seen in **Figure 5**.

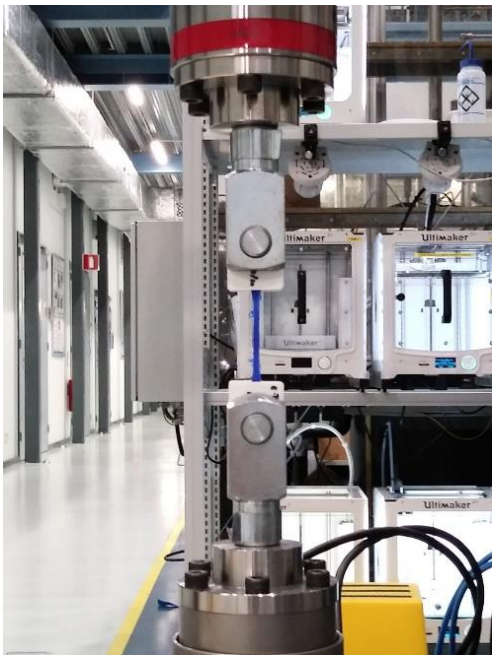

Figure 5. Experimental setups for mechanical testing. A sample of bi-material compliant mechanisms was clamped to the fixtures of the test system. This sample was subjected to the axial loading as the crosshead moving away from the base. The load cell (cylinder with red mark) above the top fixture measured the magnitude of this uniaxial force.

Fatigue testing was also conducted using the same machine and fixtures as tensile testing. Several parameters that need to be set before starting the fatigue test are stress components, stiffness, number of cycles, and frequency.

Stress components in fatigue testing consist of maximum stress (σ_{max}), minimum stress (σ_{min}), mean stress (σ_o), and the alternating stress or the amplitude (σ_a) [12, 19]. These stress components are illustrated in **Figure 6**. Determining these values are essential to ensure that the mechanisms fail only because of repetitive loading. Therefore, the maximum stress value shall not exceed the value of yield stress (σ) to avoid tensile failure [12]. The maximum and minimum stress values were determined using the measured σ, which were 80 % and 8% of σ, respectively. These values were used to calculate the values of the mean stress (σ_o) and the alternating stress (σ_a). Both values were obtained using the following equations.

$$\sigma_o = (0.8\sigma + 0.08\sigma)/2$$

$$\sigma_a = (0.8\sigma - 0.08\sigma)/2$$

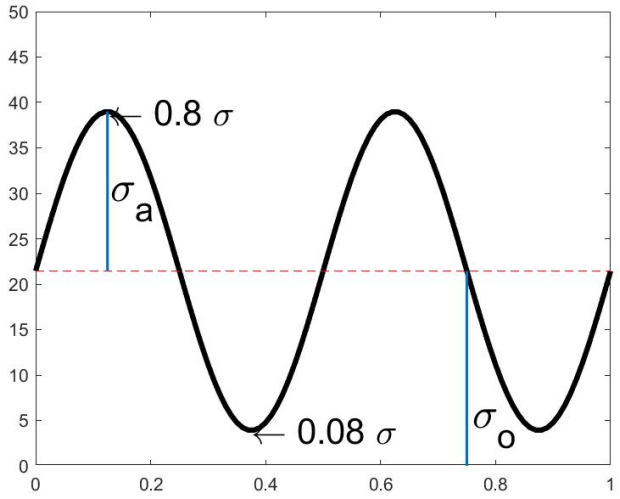

Figure 6. Stress components in cyclic loading. In this example, σ_{max} equals to 80% of yield stress (σ), and σ_{min} equals to 8% of yield stress

The stiffness values from tensile testing were used to tune the test system before starting the test. These parameters were calculated by dividing the measured yield stress and yield elongation from tensile testing. After tuning the machine, the test system was set to fluctuate the loads for 100,000 cycles. Each cycle was done every 0.5 seconds, as increasing the frequency might also increase the heat within the mechanisms.

2.7 Finite element simulation

Another approach was needed to validate the strength of the mechanisms, as the results of the mechanical evaluation were not enough to significantly distinguish materials that could be more suitable for upper-limb prosthesis application. Therefore, the finite element simulation was conducted to understand the stress concentration and to check whether the model experienced plastic deformation or fracture under certain loading case. The simulation was performed by using Abaqus (Abaqus 6.14; Simulia, RI, USA). In this simulation, a finite element model was generated for each geometry in both materials by importing parts from Solidworks to Abaqus. Each model was assumed to be homogenous. The simulation used elastic (i.e., Young's modulus) and plastic (i.e., yield stress and strain) properties from the Ultimaker datasheet in **Table 3**. However, the information of the poisson's ratio was not available in the datasheet. Therefore, it was assumed that PLA and Tough PLA had the poisson's ratio of 0.36 [30] while TPU 95A had the poisson's ratio of 0.48 [31]. After combining the parts into one assembly and attaching the beam surfaces to both clamps, one of the clamps was set to the encastre boundary condition which made this part could not move rotationally or translationally. Then, using a kinetic coupling, another clamp was connected with a reference point where the load would be applied. In this section, a boundary condition was applied to only allow the translational motion in x-axis. The load was applied at the reference point (RP) in x-direction, as can be seen in **Figure 7**. The model was meshed with tetrahedral elements. After completing all the steps, the model was simulated.

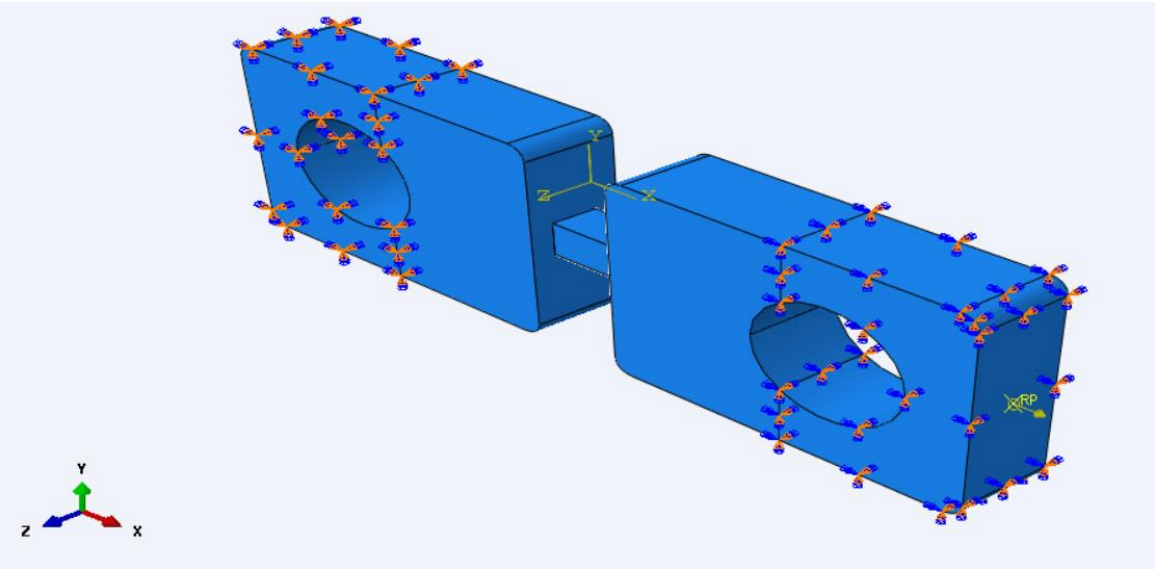

Figure 7. A schematic of constraint, boundary conditions, and loading direction for finite element simulation

Table 5. Classification of mechanisms used in tests

Group	Interface shape	Materials
A	Rectangular	PLA, TPU
B		Tough PLA, TPU
C	Cylindrical	PLA, TPU
D		Tough PLA, TPU
E	Tapered	PLA, TPU
F		Tough PLA, TPU

III. Results

3.1 Fabrication results

FDM process, along with the selected printing settings, was able to produce non-assembly bi-material compliant mechanisms with no significant defects in relatively short printing time. In this study, four samples were fabricated in each printing batch to optimize the manufacturing time. With this arrangement, the total manufacturing time for each batch was less than six hours. Each printing batch was able to produce final products with similar shape and size. The mechanisms had no visible defects, except few stringing that occurred across the clamp hole. This defect, however, was non-significant since the strings could be easily cleared in post-processing, along with the removal of support material. **Figure 8** shows the appearance of the final part at the end of post-processing.

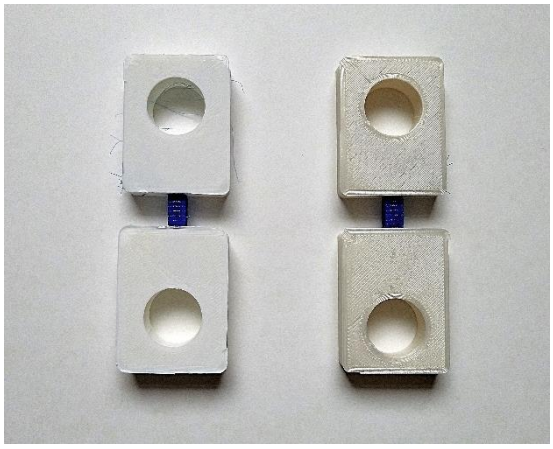

Figure 8. Bi-material compliant mechanisms with 5 mm thickness. The compliant beams were made from TPU 95A, while the clamps were fabricated with Tough PLA (left) and PLA (right). It should be noted that in the final part, it was not possible to see the geometry of the interface since the clamps were not made from the transparent material.

3.2 Tensile testing

3.2.1 Mechanisms with 0.4 mm thickness

Two samples of bi-material compliant mechanisms with 0.4 mm thickness were subjected to tensile testing. These samples consisted of one sample of the rectangular-shaped interface and one sample of the cylindrical-shaped interface, fabricated from PLA and TPU 95A filaments. Both configurations yielded after 5 N load. Using this value of yield strength, it was not ideal to conduct fatigue testing with the maximum stress of 4 N (80% of yield strength) and the minimum stress of 0.4 N (8% of yield strength). This value of minimum stress falls into the range of measurement error of the test system (0-0.5 N). In addition, the test system can give reliable measurement if the alternating loads in fatigue testing fall between 10 to 10,000 N. Therefore, it was decided that no further evaluation would be conducted regarding the behavior of the mechanisms under cyclic loading.

Despite not achieving the expected results, the tensile testing of the mechanisms with 0.4 mm thickness provided insight regarding the types of failure that might occur. Each configuration showed different kinds of failure, as shown in **Figure 9**. In the cylindrical-shaped

configuration, the fracture occurred in the middle of the compliant beam at 15 N load. However, the mechanism with rectangular-shaped interface experienced failure in the interface at 12 N load before the compliant beam reaching its breaking point. In this condition, the TPU 95A fibers of the rectangular interface were separated from the PLA fibers and slid away from one of the clamps. These two types of failures, along with the final condition of the mechanisms after tensile testing, can lead to the evaluation of contributing factors that account for the strength of the bi-material compliant mechanisms, especially at the interface between two materials.

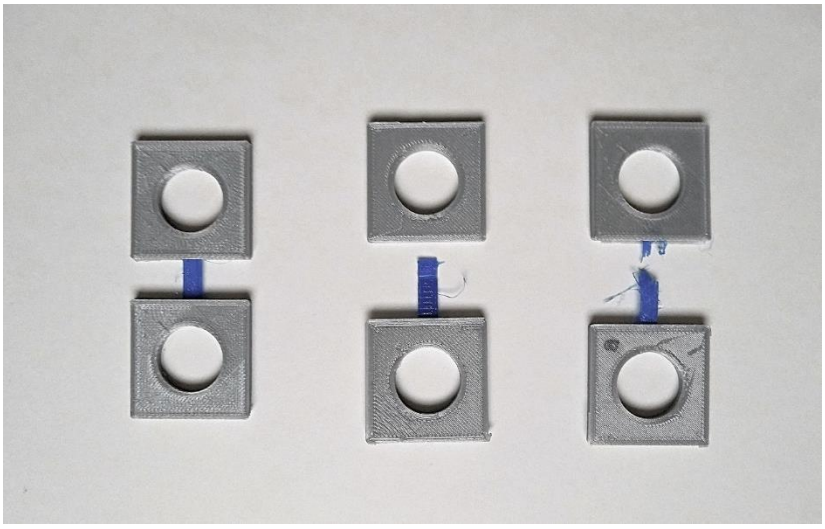

Figure 9. Comparison between mechanisms before tensile testing and after the mechanical failure. From left to right: an untested sample, a tested sample from group A (rectangular-shaped interface), and a tested sample from group C (cylindrical-shaped interface). The whole interface of a sample from group A completely slipped away from the clamp, while the interface of a sample from group C stayed inside the clamp and the mechanical failure occurred at the compliant beam.

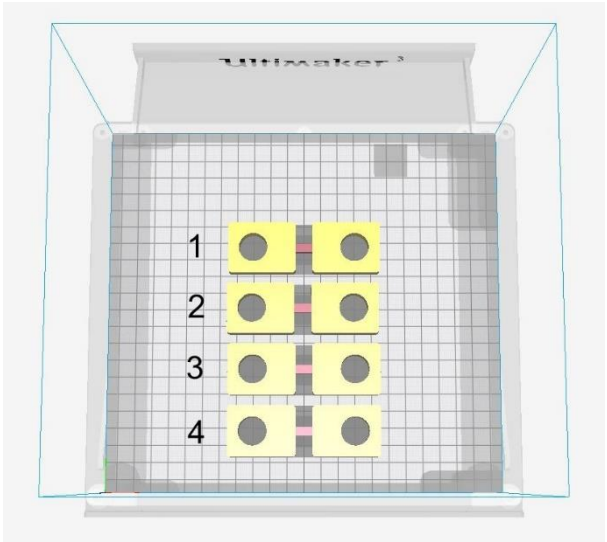

Figure 10. Sample number according to the position on the printing bed

3.2.2 Mechanisms with 5 mm thickness

For each group of the mechanisms, four samples that were fabricated in the same printing batch were subjected to the tensile testing. These samples were numbered according to their position on the printing bed, as can be seen in **Figure 10**. The example of the stress-strain curve of the mechanisms with PLA and Tough PLA can be seen in **Figure 11**. Based on these figures, mechanisms with the rectangular-shaped interface had the lowest strength while the mechanisms with the tapered-shaped interface produced the highest strength. These figures also showed that the mechanisms with the rectangular-shaped interface initially had an identical stress-strain response with the cylindrical-shaped interface before experiencing the sudden fracture.

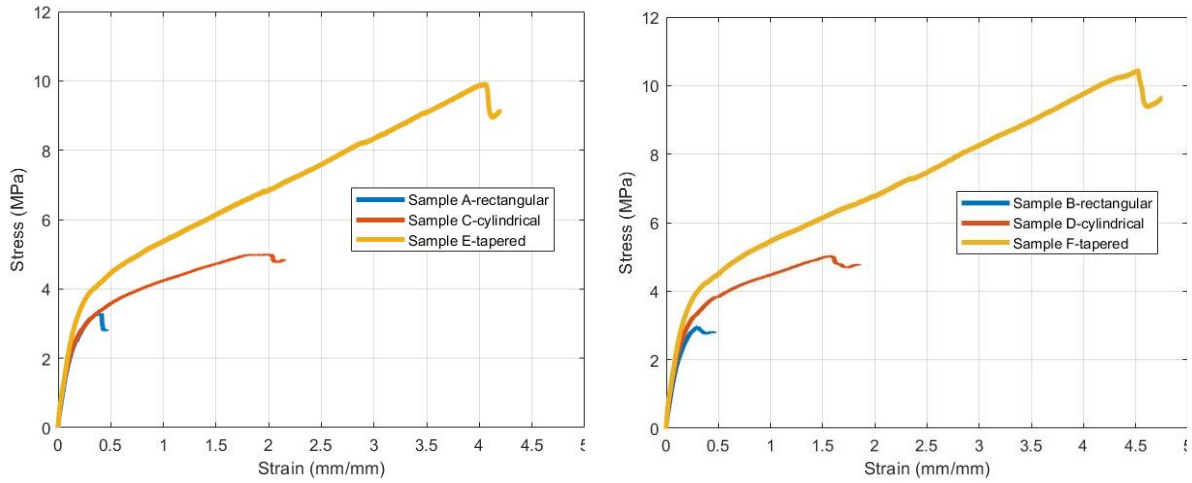

A B

Figure 11. Stress-strain curves of bi-material compliant mechanisms fabricated with TPU 95A-PLA (A) and TPU 95A-Tough PLA (B)

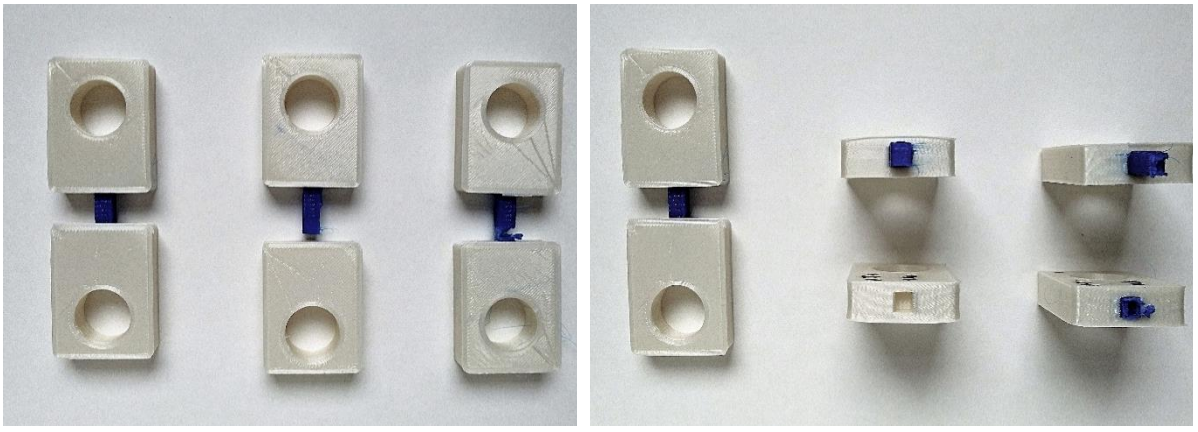

A B

Figure 12.A. Left to right: an untested sample, a tested sample from group A (rectangular-shaped interface), and a tested sample from group C (cylindrical-shaped interface). Each sample had a different mechanism of failure that can be seen in **Figure 12.B**. Similar to the mechanisms with 0.4 mm thickness, in group A, the failure occurred as the result of separation between TPU 95A and PLA layers at the interface section. In group C, the compliant beam experienced fracture.

Two types of failure mechanism were observed in this test, as can be seen in **Figure 12**. The compliant beam in each sample from all groups, except group A and B (rectangular-shaped interface), was failed before the layers at the interface showed any sign of separation. This failure mechanism was identical to the failure of the cylindrical-shaped mechanisms with 0.4 mm thickness. Samples from group A and B, however, experienced the mechanical failure at the interface, which was similar to the rectangular-shaped mechanisms with 0.4 mm thickness. The compliant beam in each sample from these groups showed no visible rupture.

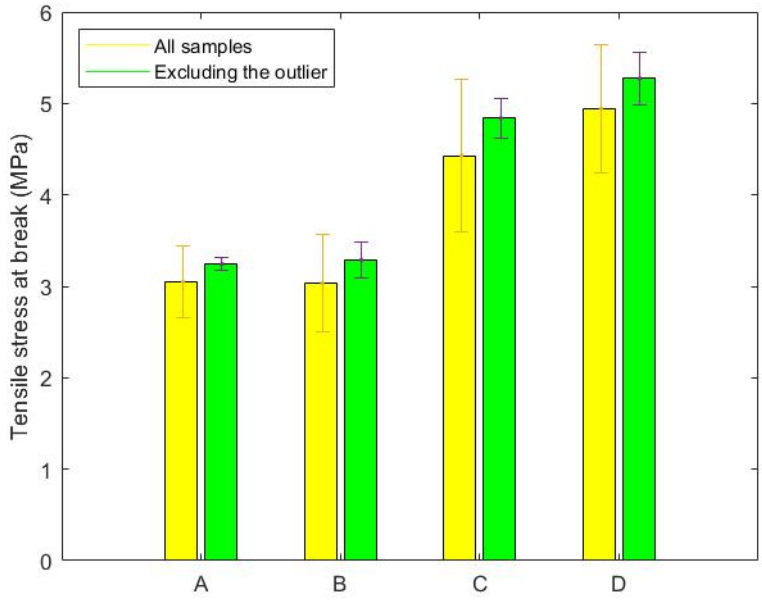

Figure 13. The average tensile stress at break of the mechanisms from group A-D

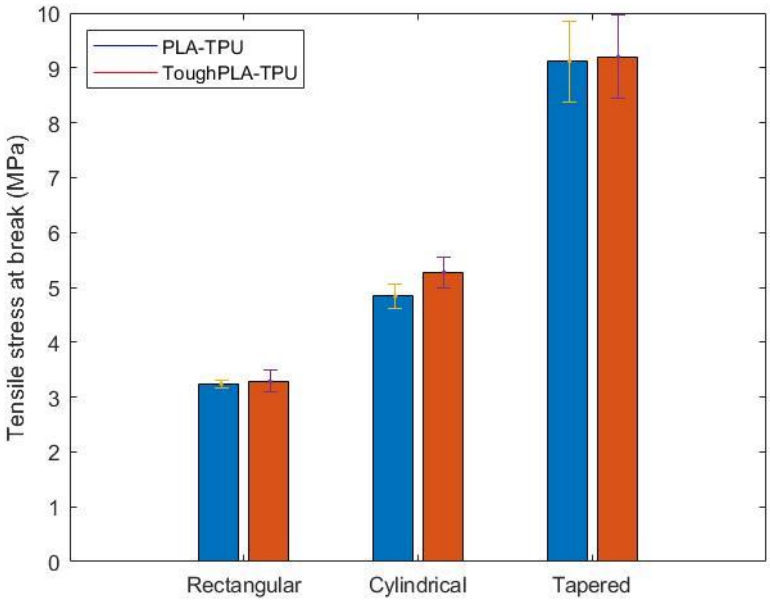

Figure 14. The average tensile stress at break of the mechanisms from all groups after excluding the outlier

In all groups except group E and F (tapered-shaped interface), it was found that there was one sample which had an inferior breaking strength value compared to the other three samples. As a consequence, the standard deviation of breaking strength in these groups are above 10%. Therefore, there was a necessity to test more samples to evaluate whether the measurement results were consistent where each sample always give similar results. After performing the additional test, it was clear that there was one sample in group A-D which always produced the deviated strength. **Figure 13** shows the average tensile stress at break for these groups with a dataset from all four samples and with a dataset that excluded one sample which gave the outlier value. In **Figure 14**, the average tensile stress at break for all groups are shown.

3.3 Fatigue testing

3.3.1 Determining maximum and minimum stress

The maximum and minimum stress of the mechanisms, which are based on the yield point, need to be determined for fatigue testing. Identifying the yield point in each mechanism in this study, however, was challenging since there was no sharp transition between elastic and plastic region. Therefore, in this study, the following methods were used to identify the yield point.

The yield point of each mechanism with the cylindrical and the tapered-shaped interface was identified according to the yield strain percentage from TPU 95A datasheet. In this estimation, the mechanisms were assumed to reach yield point at 55% strain, along with the respective stress. This value of yield strain provided sufficient estimation of the yield strength since it was observed during the test that the mechanisms with cylindrical and tapered-shaped interface experienced visible plastic deformation in form of necking around 100% of strain, suggesting that the yield point occurred beforehand.

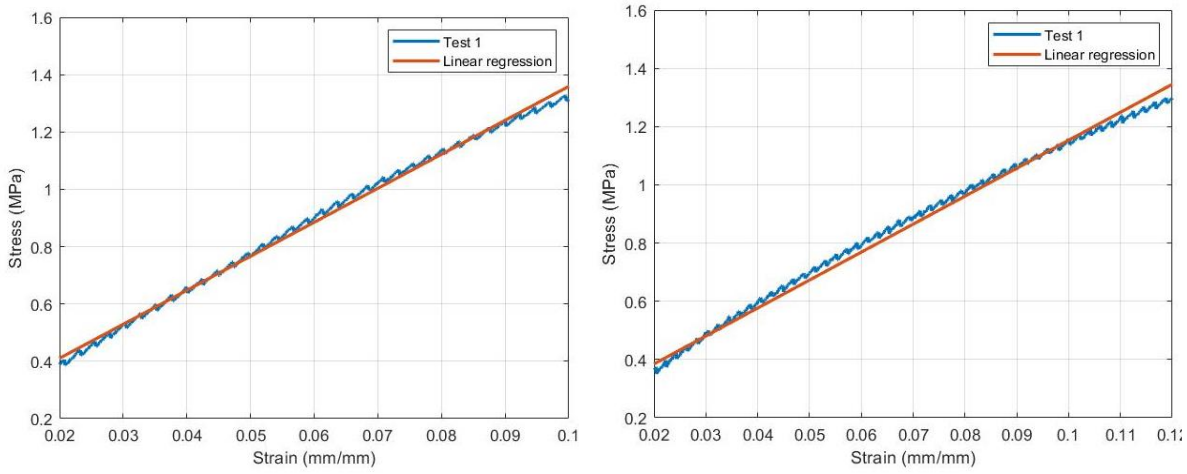

Figure 15. Stress-strain curve at the elastic region of one sample of group A (**A**) and group B (**B**)

Another approach needed to be used for mechanisms with rectangular-shaped as the mechanisms failed before reaching 55% strain. Since the compliant beam of the mechanisms did not exhibit any visible necking or fracture, it was assumed that the mechanisms failed before reaching the yield point of the compliant beam. The following approach was used for group A and B. Linear regression was made between 2-25% of strain at break (i.e. 0.08-1 mm/mm of strain for group A and 0.1-1.25 mm/mm of strain for group B) and the respective

stress. It was found that the stress-strain curves in this region had a linear behavior, as can be seen in **Figure 15**. Therefore, in this elastic region, the mechanisms would not yield, and it would be safe to use values between this region as the yield point. In this study, the yield point of these groups for fatigue testing was arbitrarily decided at 20% of strain at break in each group, which equals to 0.08 and 0.1 strain (mm/mm) for group A and B respectively, knowing that the point also fell at the elastic region.

Table 6. Stress, load, and stiffness values for fatigue testing

Group	Stress (MPa)		Corresponding load (N)		Stiffness (N/mm)
	Maximum	Minimum	Maximum	Minimum	
A	1.28	0.128	32	3.2	49
B	1.56	0.156	39	3.9	46
C	2.92	0.292	73	7.3	17
D	3.24	0.324	81	8.1	19
E	3.52	0.352	88	8.8	20
F	3.52	0.352	88	8.8	20

Figure 16 shows the average yield stress for the mechanisms for group A-D using datasets from all samples and excluding the outlier. The average yield stress for each mechanism can be found in **Figure 17**. Based on these values, the maximum and minimum stress of the mechanisms was calculated. The stiffness value for each group was also calculated by dividing load and deformation at yield point. **Table 6** shows the values of maximum and minimum stress, the corresponding values of maximum and minimum load, and the stiffness of each group, that were used for fatigue testing.

3.3.2 Fatigue testing results

In this study, three series of fatigue testing were conducted. The tests consisted of the main experiment and other two additional measurements to validate the method of determining the yield point and the exclusion of the sample. The results from these tests are explained in this section.

A pilot experiment was performed to confirm the validity of the selected method for yield point determination. In this experiment, one sample each from group A-D were tested under cyclic loading with the corresponding values of maximum and minimum stress. All samples could finish 100,000 cycles. Therefore, it was decided to keep using the obtained yield point for the subsequent fatigue testing.

Another experiment was also conducted to investigate whether the specific sample which produced outlier value of strength could withstand the cyclic loading with the selected maximum value. This experiment was performed using the inferior sample from group C and D. The sample from group C failed after 1,496 cycles while the one from group D experienced a fracture at the 604th cycle. Based on this result, it was decided to exclude the inferior sample

from each group for the fatigue experiment. Even though this pilot experiment did not use any sample from group A and B, it was also decided to remove the outlier sample from both groups to have better confidence in fatigue testing.

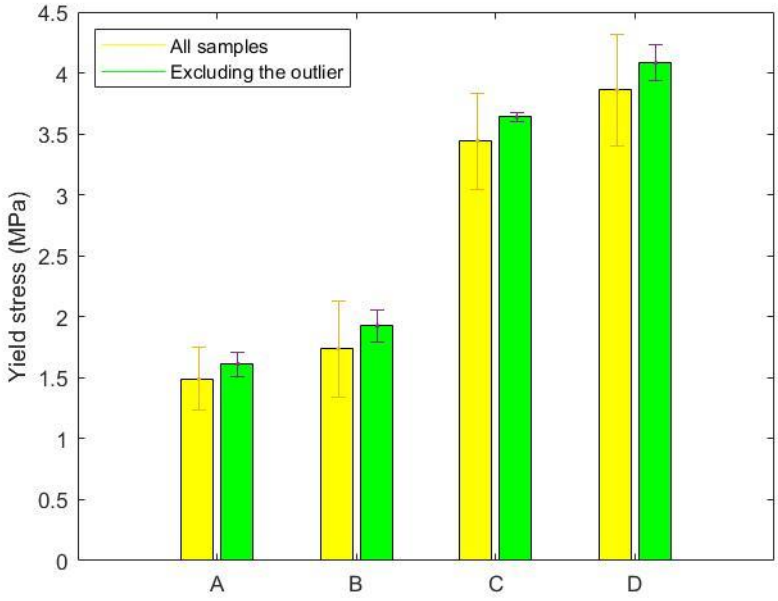

Figure 16. The average yield stress of the mechanisms from group A-D

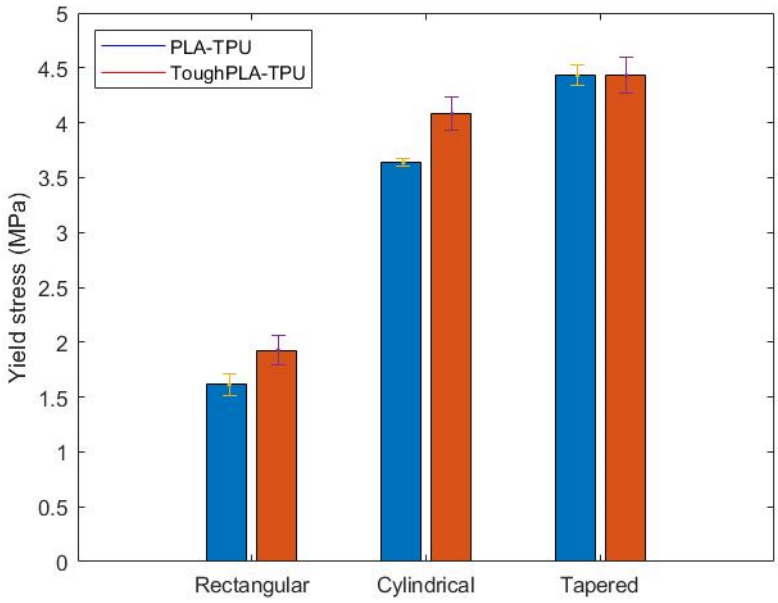

Figure 17. The average yield stress of the mechanisms from all groups after excluding the outlier

The main experiment consisted of testing three samples from each group. All samples in group A and B completed 100,000 cycles without any visible rupture. However, samples from other groups which were subjected to the higher load experienced mechanical failure before finishing 100,000 cycles. Despite the sample from the pilot experiment of group C was able to complete 100,000 cycles, the maximum cycle that could be reached in this main experiment was 50,683

cycles while another sample could only achieve 46,792 cycles. Group D, which had the same geometry but fabricated with Tough PLA instead of PLA, showed inferior results compared to group C. In this group, the range of the completed cycle fell between 7,079-8,667. In the mechanisms with a tapered-shaped interface, the results were more scattered. The minimum cycle that could be achieved before the failure occurred in group E and F was 28,993 and 16,460, respectively. However, the maximum cycle could reach 52,965 for a sample in group E and 100,000 for another sample in group F. These results produced the high standard deviation in both groups, especially group F. **Table 7** provides the detail results of cycles completed by each sample in all groups. The average values of the number of cycles completed in each group are shown in **Figure 18**.

Table 7. Fatigue testing results

Group	Cycles completed			Average cycles completed	Standard deviation (%)
A	100,000	100,000	100,000	100,000	0
B	100,000	100,000	100,000	100,000	0
C	50,683	46,792	49,048	48,841	4
D	8,322	8,667	7,079	8,023	10
E	28,993	47,130	52,965	43,029	29
F	28,428	100,000	16,460	45,175	93

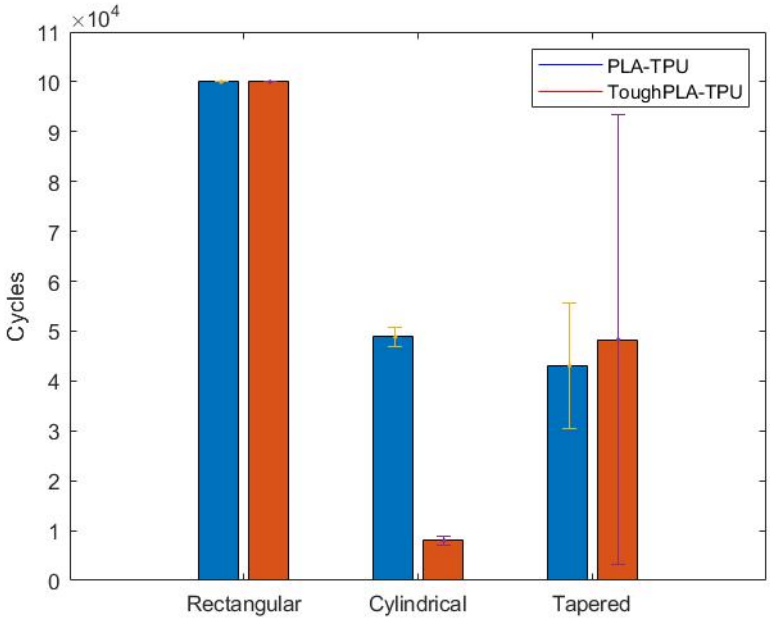

Figure 18. The average completed cycles in each group

3.4 Finite element analysis

The results of tensile and fatigue testing have limitations in several areas. First, both tests could not provide further insight regarding the stress concentration within the mechanisms under certain loading case. Furthermore, the results of tensile stress indicate that with similar geometry, both material configurations presented comparable values of tensile stress at break as well as at yield. Hence, it was not feasible to observe which material configurations could offer better strength. In addition, the observation of large deviation on cycles completed in fatigue testing emerged another concern to provide more validation whether the early failure was due to repetitive loading or the applied stress was not on the elastic region which caused the sudden fracture before reaching the expected number of cycles completed.

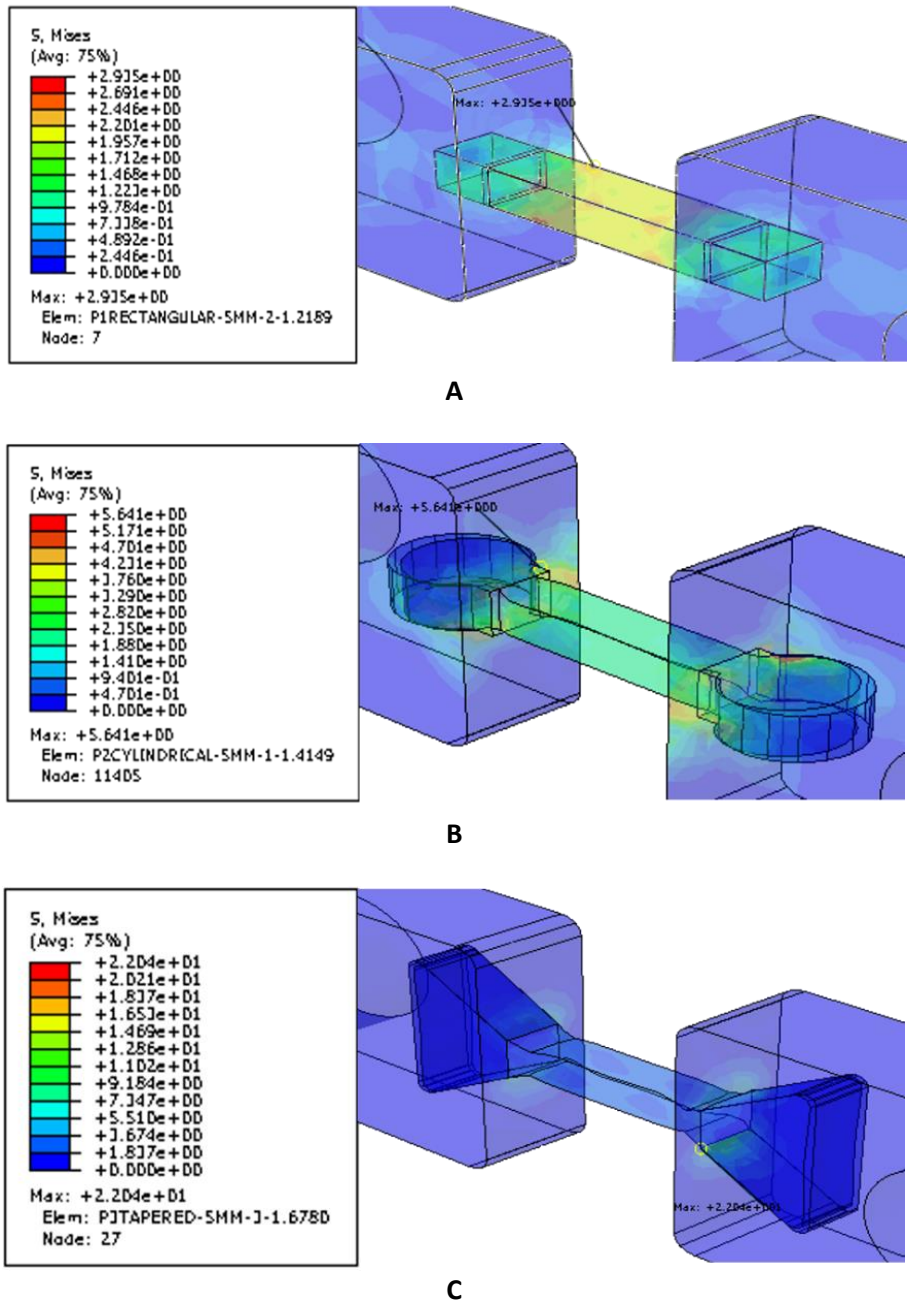

Figure 19. Von Mises stress distribution of the PLA-TPU95A mechanisms with (A) rectangular, (B) cylindrical, and (C) tapered-shaped interface under axial loading of 50 N

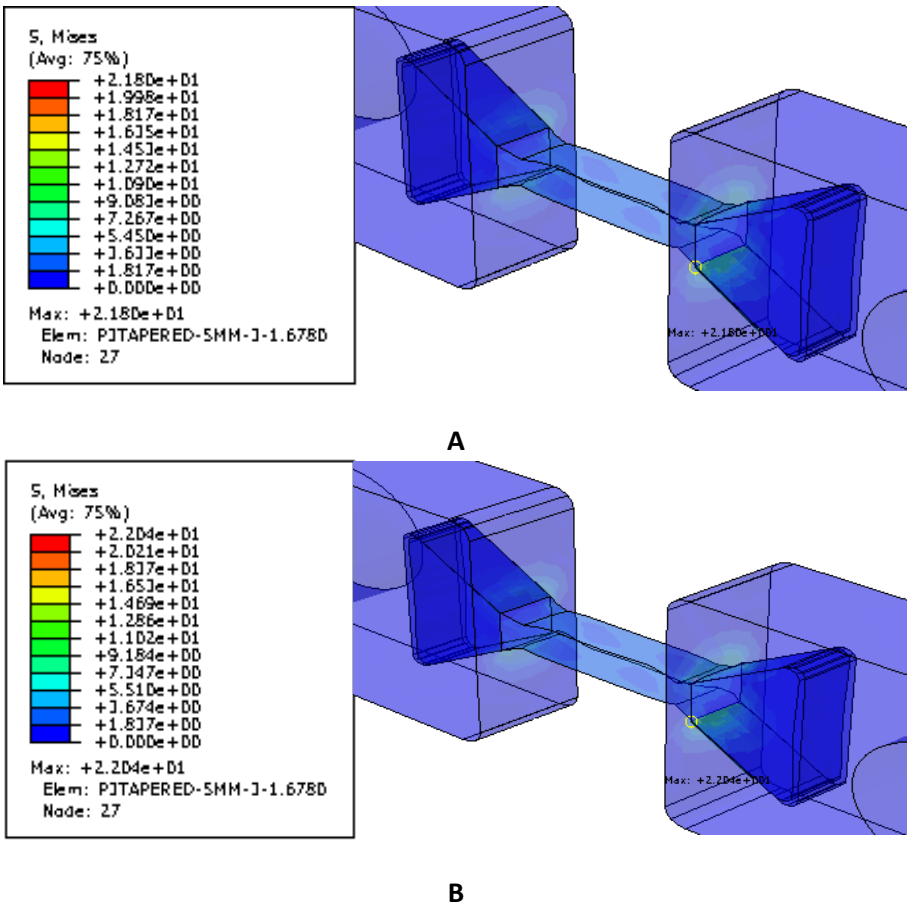

Figure 20. Von Mises stress distribution of the mechanisms with tapered-shaped interface under axial loading of 50 N. The model was simulated using different materials: A. PLA-TPU95A, and B. Tough PLA-TPU95A

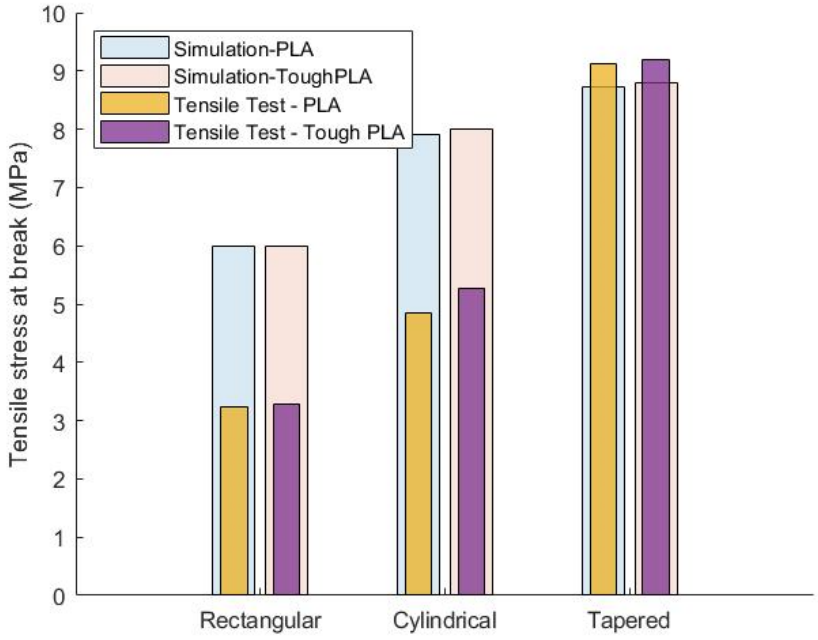

Figure 21. Breaking stress of the mechanisms according to the results of tensile test and simulation

The results of finite element simulation addressed the aforementioned problems. All mechanisms in 5 mm thickness were simulated using axial loading of 50 N. The comparison of stress distribution of geometries fabricated with PLA-TPU 95A can be seen in **Figure 19**. Based on this figure, it was found that the force is more evenly distributed in the tapered-shaped geometry. The stress distribution results of mechanisms simulated with Tough PLA-TPU 95A are shown in **Appendix C**. In similar geometry, the stress distribution on the finite element model simulated with PLA-TPU 95A is comparable with another model made with Tough PLA-TPU 95A. As an example, **Figure 20** shows the comparison of the stress distribution between both material configurations in tapered-shaped interface. The comparison of both material configurations in other geometries can be found in **Appendix D**.

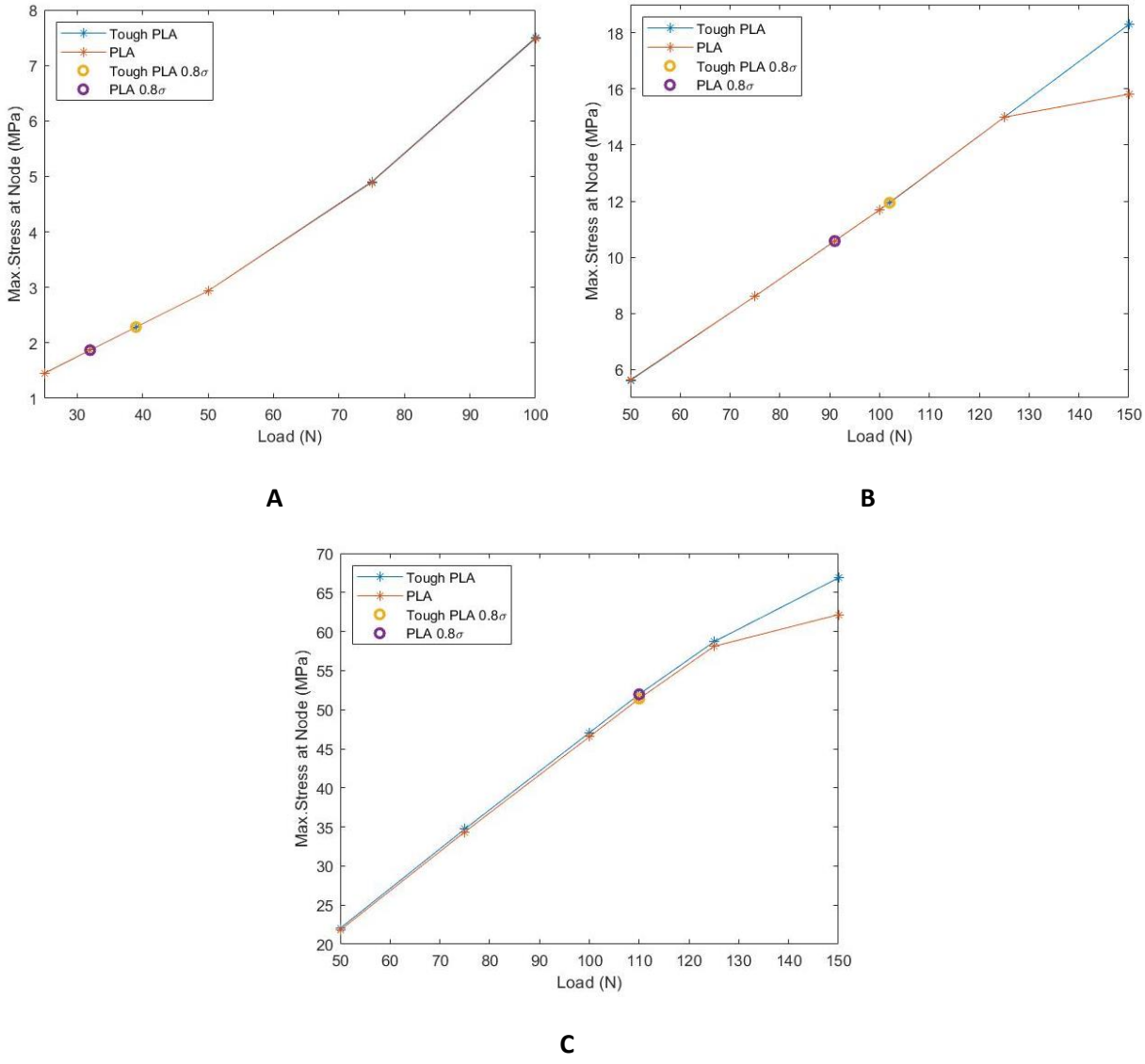

Figure 22. Stress-load curve of each model from finite element simulation.
A. Rectangular. B. Cylindrical. C. Tapered-shaped interface

Further evaluations of fracture and the elastic region of each model were performed in this simulation. First, the model was subjected to several loading cases to find the breaking point. The comparison between the breaking strength of the mechanisms according to tensile test and simulation can be found in **Figure 21**. **Appendix E** shows the fracture condition of each model

according to the simulation. Then, the assessment of the elastic region was conducted. At least four different loading cases were simulated. The resulted maximum stresses were plotted against the loads. As the stress is proportional to load, the linear region in this graph also represents the elastic region with no plastic deformation that can affect the linearity of the graph. To investigate whether the selected load for fatigue testing was within the elastic region, this load was also simulated and plotted on the previous stress-load curve. **Figure 22** shows the plot of stress-load in this simulation, which also shows that all the selected loads for fatigue testing are within the elastic region. The list of selected loads, as well as the results of Von Mises stress and strain from each simulation can be found in **Appendix F**.

4. Discussion

This study analyzed the mechanical characteristics of different geometries of non-assembly bi-material compliant mechanisms. The mechanisms consist of parts made from two different materials which served as flexible and rigid components. FDM was used to fabricate the mechanisms in a single step. The mechanisms were subjected to static and dynamic tests to understand the strength and fatigue behaviors of the mechanisms further. Finite element simulation was used to investigate the stress concentration and to validate the results of mechanical testing. In this chapter, evaluation of printing parameters, strength and fatigue behavior of the mechanisms, as well as challenges and future work are presented.

4.1 Evaluation of printing parameters

During the fabrication step, TPU 95A filaments and PLA or Tough PLA were extruded using two different nozzles. At first, default printing parameters were used to fabricate the bi-material compliant mechanisms. However, several problems occurred while printing, such as separation of the part from the building plate while printing, cracks, layer misalignment, and stringing, to name a few. Therefore, key parameters were adjusted one at a time to obtain the optimum settings.

Few modifications were made to the PLA and Tough PLA settings to have a better attachment of part to the printing bed and to increase the ease of post-processing step. The extruder was set to print extra layers in the form of brim with relatively large width. This build plate adhesion helped the fabricated component to stick to the printing bed without damaging the bottom area. In addition, the PLA and Tough PLA was also set as the support material for the whole mechanisms instead of using TPU 95A. While experimenting with TPU 95A as the support material, the compliant beam completely fused to the support structure, which increased the difficulty of removing support material. By using PLA or Tough PLA, the support structure could be peeled off easily from the compliant beam.

As most printing problems happened while printing the compliant beam, major adjustments of printing parameters were made to TPU 95A printing settings. Reducing the printing speed and travel speed from the recommended values could help each layer to bond more precise to the adjacent layers, which prevent cracks and layer misalignment. These settings were also supported with increasing the minimum layer time to ensure each layer could sufficiently cool down and set. Modification of the infill density parameter was also made. The initial setting of printing TPU 95A according to Ultimaker Cura is by using a high value of infill density with gradual infill steps, which means the top layer will have the highest density while the density of the lower layers will gradually decrease. In this study, it was decided to change this variable to the constant infill density for all sections to produce a homogenous part.

Despite successfully fabricating the mechanisms in one step without further assemble and extensive post-processing, the selected combination of printing parameters could not result in mechanisms with the expected yield and breaking strength. **Table 8** shows the comparison between the yield strength according to the technical data sheet and the results of tensile testing. Increasing the infill density has the potential to improve the strength of the mechanisms. However, this parameter should also be carefully assessed since it would also increase the printing time and the total amount of material use.

Table 8. Comparison of yield strength values

	Technical Data Sheet [29]	Group A	Group B	Group C	Group D	Group E	Group F
Yield Strength (MPa)	8.6	1.61 ± 0.10	1.93 ± 0.13	3.63 ± 0.03	4.08 ± 0.15	4.43 ± 0.09	4.43 ± 0.17

4.2 Geometry comparison

4.2.1 Strength evaluation

According to the results of tensile testing and finite element simulation, the mechanisms with tapered-shaped interface achieved the highest value of yield and breaking strength while the mechanisms with rectangular-shaped interface had the weakest strength among all groups. Several geometry factors affected these results, including the dimension of the interface, the relation between the size of the cross-sectional area of the interface and the clamp slot, and the stress concentration around discontinuities.

As the bond strength of dissimilar materials is considered inferior to the bond of similar materials [10, 11], special attention should be given to the interface between two materials. In this weak point, the dimension of the interface could affect the strength of the mechanisms. A larger surface area of the interface indicates more layers of TPU 95A are deposited on the top of PLA or Tough PLA layer. Increasing the number of layers that are well-bonded to each other at this interface section contributes to the higher strength of the mechanisms. Therefore, despite having the similar initial response to static loading, the mechanisms with the cylindrical-shaped interface could withstand further loading as opposed to the mechanisms with the rectangular-shaped interface which had a smaller surface area.

The relation between the size of the cross-sectional area of the interface and the clamp slot also holds an important function in achieving the high-strength bi-material compliant mechanisms. The cross-section area of the rectangular-shaped interface and the clamp slot are in the same dimension. It was found that with this similar dimension, when the separation of TPU 95A and PLA/Tough PLA layers occurred, the whole interface section inside the clamp could easily escape through the clamp slot. However, in the cylindrical and tapered-shaped interface, the cross-section area of the clamp slot was smaller than the interface. This smaller dimension of the clamp slot prevented the larger component from slipping away. Even though the separation of TPU 95A and rigid materials already started, the mechanisms did not instantly break as the component of TPU 95A inside the clamp were still well-bonded and could not escape from the smaller clamp slot. Therefore, the mechanisms could withstand a higher load until the TPU 95A layers yielded, which subsequently led to plastic deformation and mechanical failure at the compliant beam.

Geometric discontinuity affects the mechanical behavior of the mechanisms. Mechanisms that are fabricated with ductile materials can easily fracture as if they are made from brittle materials if the sharp discontinuities present in the mechanisms, which increase the stress concentration around these sudden changes of geometry. Smooth transition in the geometry, with the application of tapering or filleting method, could reduce the stress concentration which results

in a stronger mechanism [19]. In this study, it was observed that the mechanisms with sharp discontinuities (i.e., the rectangular and cylindrical-shaped interface) had a lower breaking strength than the mechanisms with the tapered-shaped interface. Further observation on the stress concentration from finite element simulation of each geometry under similar loading condition is beneficial to understand the effect of geometric discontinuity. The results of the simulation show that high localized stress area occurs near the sharp corners of the rectangular interface as opposed to evenly stress distribution on the tapered-shaped interface. Therefore, the rectangular design is more prone to early failure as the localized stress area can initiate early crack that further propagates.

Overall, the mechanisms with tapered-shaped interface present a promising result to be utilized in upper-limb prosthesis as these mechanisms presented the highest strength and more evenly stress distribution compared to other designs. Furthermore, each tested sample of the tapered-shaped design could produce strength value that is relatively close to each other and contributes to a relatively low standard deviation without the need of excluding any sample from the measurement. However, there are still many possible geometries that could be adapted into bi-material compliant mechanisms. For example, instead of using tapered geometry, other types of smooth transition such as fillet could also produce the mechanism with a high value of yield and breaking strength. Nevertheless, the assessment of three different geometries in this study provided the applicable strategies to increase the strength characteristic of the FDM-fabricated bi-material compliant mechanisms.

4.2.2 Fatigue behavior

Analyzing the fatigue behavior of the bi-material compliant mechanisms is as important as evaluating the strength of the mechanisms. It would be impractical to use the mechanisms for the upper-limb prosthesis if the fatigue failure occurred before reaching the expected period of use. This section presents the analysis of fatigue behavior of the mechanisms with different geometry.

The results of fatigue testing show that only the mechanisms with the rectangular-shaped interface could withstand 100,000 cycles. The rectangular-shaped interface was subjected to a relatively low alternating load compared to other mechanisms. This result indicated that with this range of load, there was no significant microfracture that could lead to mechanical failure in the mechanisms. Other mechanisms, however, failed before reaching the expected number of cycles. It was observed that the mechanisms had plastic deformation before showing any visible ruptures.

The permanent change of the shape of the compliant beam and the mechanical failure of the mechanisms with the cylindrical and tapered-shaped interface before reaching 100,000 cycles could be interpreted as follows. First, the characteristics of TPU needs to be taken into account. The microstructure of TPU consists of hard segments of thermoplastic polymer bonded with soft parts which have rubbery behavior [31]. With this two-phase microstructure, TPU has both thermoplastic and elastomer properties [32]. Interactions between thermoplastic and elastomer segments, as well as other internal factors in each segment, contribute to the energy dissipation of the TPU. Having energy dissipation contributes to the viscoelasticity of TPU, where the stress-strain behavior is time-dependent. Therefore, the mechanisms that are fabricated with TPU needs stress relaxation time to be back to the initial state after subjected to certain loading [31, 33]. In this study, the test system alternating the load from maximum to minimum using corresponding values of stiffness coefficient and displacement in 0.5 seconds, since the frequency for cyclic loading was set to 2 Hz. In the mechanisms with the rectangular-shaped

interface, this frequency was suitable to alternate the load and the corresponding displacement between 3.2-3.2 N and 0.065-0.65 mm for PLA-TPU 95A configuration and 3.9-39 N and 0.083-0.83 mm for Tough PLA-TPU95A configuration without plastic deformation. Other geometries, however, were subjected to higher alternating load and displacement which lead to time-dependent deformation. For example, the cyclic load for the mechanisms with tapered-shaped interface fabricated from PLA and TPU 95A was alternating between 8.8-88 N while the deformation range was 0.44-4.4 mm. In this case, the mechanisms were continuously experiencing cyclic loading under selected frequency before completely reaching the initial state at 0 mm deformation. The deformation gradually becomes permanent which contributes to mechanical failure. In addition, the chosen frequency might also increase the friction and heat within the mechanisms, which also affect the crack propagation.

Despite not completing the expected cycles, both cylindrical and tapered-shaped interface are still preferable than the rectangular-shaped interface. As the stress-strain curve of the mechanisms shows that the elastic region of the rectangular-shaped interface also falls in the elastic region of other mechanisms, both cylindrical and tapered-shaped interface could also achieve 100,000 cycles if they were tested under similar alternating load and displacement that were used for the rectangular-shaped interface. Furthermore, changing the testing parameter, especially the frequency, could be beneficial to assess the durability of the mechanisms under the proposed cyclic load without generating fracture within the mechanisms.

4.3 Material selection

A wide range of materials that are applicable for FDM technique expands the opportunities to select the suitable combination for fabricating bi-material compliant mechanisms. The selected materials need to fulfill the strength and durability requirements. However, choosing a specific material that can strongly bond with another type of material is relatively complex since there are a lot of factors that affect the bond strength between dissimilar materials, including the type of bonding method and the differences in the physical and chemical properties of materials [11]. In this study, it was not feasible to accurately predict the bonding behavior between the materials, as limited literature was found regarding physical and chemical properties of Ultimaker PLA, Tough PLA, and TPU 95A. Therefore, further assessment of the bonding behavior between the materials could not be conducted. Instead, the evaluation to determine which selected materials that have potential for the upper-limb prosthesis application is discussed in this section by comparing the results of mechanical testing and finite element simulation.

Based on the tensile testing results, Tough PLA produced a slightly stronger mechanism compared to PLA. The highest difference in the breaking strength was observed in the cylindrical design where the average breaking stress of Tough PLA samples was 9% higher than the PLA samples. The average breaking stress value for Tough PLA samples from other geometries, however, were only 1.3% and 0.9% higher for rectangular and tapered-shaped group, respectively. In terms of the selected stress values for fatigue testing that was derived from the tensile testing results, a wider divergence was observed. Despite both Tough PLA and PLA samples in tapered-shaped group had similar values, Tough PLA samples resulted in 10% and 22% higher limit for fatigue testing than PLA samples in rectangular and cylindrical group, respectively.

The finite element simulation showed that both PLA and Tough PLA models with similar geometry had an identical stress distribution. However, each material generated different value

of maximum von Mises stress. By plotting the maximum von Mises stress values under various loads, the elastic characteristic of each model could be compared. According to the plot of maximum von Mises stresses against loads in the simulation of cylindrical and tapered-shaped interface, the slope of the PLA curve changed after subjected to 125 N of load while the Tough PLA curve remained linear. This linearity change indicates that the transition from elastic to plastic region was occurred in the PLA model, where it also started to deform plastically earlier than the Tough PLA model. Therefore, with a higher elastic limit, the Tough PLA model could be subjected to a higher load compared to the PLA model with no plastic deformation.

Despite a stronger mechanism could be fabricated by selecting Tough PLA rather than PLA, additional review was needed to examine its durability. According to the results of fatigue testing, it was found that all samples from both PLA and Tough PLA group could complete 100,000 cycles. Although the Tough PLA samples could complete the cycles 5% higher than the PLA samples in tapered-shaped design, the completed cycles in PLA samples was six times higher than the Tough PLA samples. Moreover, the standard deviation of cycles completed were higher for the Tough PLA mechanisms in both cylindrical and tapered-shaped design, compared to the Tough PLA mechanisms. This result indicates that the melting-solidification process of PLA and TPU 95A in each fabrication was more consistent than the combination of Tough PLA and TPU 95A. Hence, the PLA mechanisms gave better certainty for constructing the mechanisms where each fabricated sample could demonstrate the relatively similar cyclic loading behavior.

To summarize, the combination of Tough PLA and TPU 95A produced a stronger mechanism compared to PLA-TPU 95A in similar geometry. Meanwhile, PLA-TPU 95A was able to give better reliability in terms of producing consistent strength and durability throughout the whole tested samples. Since both Tough PLA and PLA mechanisms could fulfill the strength requirement of withstanding at least 67 N of load in cylindrical and tapered-shaped geometry, the combination of PLA-TPU 95A that produced mechanism with better durability would be more suitable for the upper-limb prosthesis application.

4.4 Challenges and future work

Several challenges presented while conducting fabrication and mechanical evaluation of the bi-material compliant mechanisms that were fabricated using the FDM process in a single step. Therefore, recommendations are proposed for further evaluation, including the optimization of printing parameters, geometry, material, finite element simulation, and testing setup.

The optimization method of printing parameters faced several limitations. As a relatively new technology, there are currently no specific guidelines to select the suitable combination of the FDM printing parameters. Therefore, in this study, the particular values of modified printing parameters were arbitrarily determined, and the process was also conducted with trial and error. During optimization, the external factors such as ambient temperature and humidity that also influenced the printing result were ignored. Another challenge is to understand the impact of changing one setting on the other. Choosing a specific value for a parameter might influence other parameters, as printing parameters are interdependent. However, the interdependency behavior of printing parameters is out of the scope of this study and presents an opportunity to be investigated in future research.

This experiment was only able to evaluate three different geometry of the interface. After investigating the current designs, it was found that increasing the dimension of the interface,

designing a clamp slot with a smaller cross-section area than the interface, and avoiding geometry discontinuities have potential to be applied in the further design of bi-material compliant mechanisms. Furthermore, exploring the strength and fatigue behavior of various configuration of compliant mechanisms such as using a corrugated compliant beam or other beam-based geometry that have a spring-like characteristic as the flexible part could also provide more guidelines in designing the mechanisms.

Regarding the selection of material, FDM has an advantage of providing various compatible polymers which present a prospective modification of the current design. For example, using the transparent PLA filament for the rigid parts could be more suited than the colored filament to have a clear observation on the separation of TPU 95A layers from the PLA layers inside the clamp. Furthermore, it would also be beneficial to assess the behavior of the different combination of materials other than two combinations that were used in this study to provide more alternatives in fabricating the mechanisms.

Each finite element model in this study was assumed as an assembly of three isotropic, homogenous parts (i.e., two clamps and one beam) while the actual parts consisted of many anisotropic filaments. Therefore, it was not applicable to analyze the viscoelastic behavior and to predict the bond strength of the filaments, especially at the interface area. These inabilities are also the shortcomings in this study. Hence, there are several recommendations to improve the finite element simulation. Using a model that consists of several layers of material is recommended to understand the behavior of each layer, especially during the separation after being subjected to a certain load. Although more effort is needed to simulate the actual FDM part with many filaments, simplification could be made by assuming all filaments in each layer are well-bonded to each other, creating a homogenous sheet. As the viscoelastic data of the FDM materials are currently not available, it is also necessary to fill the gaps by conducting more studies to define the viscoelastic properties that can be beneficial for future simulation.

Another limitation of this study is the optimization of the testing setup. First, it would be advantageous to set the testing system to investigate not only the effect of axial loading but also the bending moment, since the kinematic of upper-limb prosthesis also involving bending behavior. Since the selected fatigue testing frequency might not be suitable for testing component fabricated from the material that need a certain amount of stress relaxation time, a lower frequency should be utilized in the next study to have a better comparison between various designs. In addition, an additional step is recommended to give better understanding regarding the early plastic deformation and failure issues that occurred before reaching the expected cycles. In this step, the sample needs to be removed from the fatigue testing after certain cycles and would be subjected to a tensile test to check its elasticity. For example, if the elastic behavior of the sample that completed 10,000 cycles is identical to another sample that was not subjected to fatigue testing, this result validates that no permanent deformation occurred at 10,000 cycles. By repeating this step with another sample that completed different cycles, the cycles where the mechanisms started to demonstrate plastic deformation could be estimated.

5. Conclusion

This study presents the mechanical evaluation of six groups of bi-material compliant mechanisms where each mechanism consisted of a flexible beam and two rigid clamps. Based on the shape of the interface section between the beam and the clamps, there were three different configurations of the mechanisms: rectangular, cylindrical, and tapered-shaped interface. FDM process was used to fabricate all mechanisms without further assembly. TPU 95A was used for the flexible beam while the clamps were made from PLA or Tough PLA in each design. The Instron ElectroPuls™ E10000 Test System was used in both tensile testing and fatigue testing to evaluate the strength and fatigue of all groups. Two important criteria were used to assess the feasibility of using the mechanisms for the upper-limb prosthesis: the mechanisms need to withstand at least 67 N of load and 100,000 of cyclic loading. Based on the results of tensile testing which were also validated with the finite element simulation, both materials combinations fulfilled the strength requirement. The combination of Tough PLA and TPU 95A could produce mechanisms with a slightly higher strength compared to PLA-TPU 95A. In fatigue testing, however, it was found that PLA-TPU 95A mechanisms were more durable than Tough PLA-TPU 95A by completing more cycles with relatively low standard deviation. Hence, PLA-TPU 95A combination was more suitable to be utilized in the upper-limb prosthesis. In terms of geometry, the strength of the tapered-shaped interface was clearly more superior in comparison with others. Both cylindrical and tapered-shaped designs were able to fulfill the strength requirement. However, these geometries experienced fracture before reaching the expected number of cycles in fatigue testing. Several factors could have affected this early mechanical failure such as limitations in fabricating identical samples and the relatively high frequency of fatigue testing. The optimization of printing parameters and testing setup needs further evaluation. Other improvements that could be conducted in future studies are including, but not limited to, analyzing the viscoelastic behavior of the mechanisms, using different geometry and material selections, and performing further investigation of the mechanisms under bending condition.

References

1. Bijadi, S., et al., *Application of Multi-Material 3D Printing for Improved Functionality and Modularity of Open Source Low-Cost Prosthetics: A Case Study.* 2017(40672): p. V001T10A003.
2. Howell, L.L., *Compliant mechanisms*. 2001, New York: John Wiley & Sons.
3. Machekposhti, D.F., N. Tolou, and J.L. Herder, *A Review on Compliant Joints and Rigid-Body Constant Velocity Universal Joints Toward the Design of Compliant Homokinetic Couplings.* Journal of mechanical design., 2015. **137**(3): p. 032301-032301.
4. Mutlu, R., et al., *3D Printed Flexure Hinges for Soft Monolithic Prosthetic Fingers.* Soft Robotics, 2016. **3**(3): p. 13.
5. Gouker, R.M., et al., *Manufacturing of multi-material compliant mechanisms using multi-material molding.* The International Journal of Advanced Manufacturing Technology, 2006. **30**(11): p. 1049-1075.
6. Conner, B.P., et al., *Making sense of 3-D printing: Creating a map of additive manufacturing products and services.* Additive Manufacturing, 2014. **1–4**: p. 64-76.
7. Gibson, I., D. Rosen, and B. Stucker, *Additive Manufacturing Technologies 3D Printing, Rapid Prototyping, and Direct Digital Manufacturing.* 2015.
8. Cuellar, J.S., et al., *Additive manufacturing of non-assembly mechanisms.* Additive Manufacturing, 2018. **21**: p. 150-158.
9. Espalin, D., et al., *Analysis of Bonding Methods for FDM-Manufactured Parts.* 21st Annual International Solid Freeform Fabrication Symposium - An Additive Manufacturing Conference, SFF 2010, 2010: p. 11.
10. Yin, J., et al., *Interfacial bonding during multi-material fused deposition modeling (FDM) process due to inter-molecular diffusion.* Materials & Design, 2018. **150**: p. 104-112.
11. Vaezi, M., et al., *Multiple material additive manufacturing – Part 1: a review.* Virtual and Physical Prototyping, 2013. **8**(1): p. 19-50.
12. Gere, J.M. and B.J. Goodno, *Mechanics of Materials*. 2012: Cengage Learning.
13. Chowdhury, P. and H. Sehitoglu, *Mechanisms of fatigue crack growth – a critical digest of theoretical developments.* Fatigue & Fracture of Engineering Materials & Structures, 2016. **39**(6): p. 652-674.
14. Kutz, M., *Standard handbook of biomedical engineering and design*. 2006, New York: McGraw-Hill.
15. Luchetti, M., et al., *Impact of Michelangelo prosthetic hand: Findings from a crossover longitudinal study.* J Rehabil Res Dev, 2015. **52**(5): p. 605-18.
16. Cordella, F., et al., *Literature Review on Needs of Upper Limb Prosthesis Users.* Frontiers in Neuroscience, 2016. **10**(209).
17. NEN, *Dutch adults, DINED Dataset 1982*. 1982.
18. Alexander, B. and V. Kotiuk, *Proportions of Hand Segments.* International Journal of Morphology, 2010. **28**: p. 4.
19. Peterson, R.E., *Stress Concentration Factors*. 1974, New York: John Wiley & Sons.
20. van der Kroft, M.C., *The Hybrid Finger: Combining Nature with Technology into a 3D Printed Finger for a Hand Prosthesis with Minimized Assembly*, in *Mechanical Engineering*. 2018, Delft University of Technology: Delft.
21. Ready, S., G. Whiting, and T.-N. Ng, *Multi-Material 3D Printing.* NIP & Digital Fabrication Conference, 2014.
22. Steutel, P., G.A. Kragten, and J.L. Herder, *Design of an Underactuated Finger With a Monolithic Structure and Largely Distributed Compliance.* 2010(44106): p. 355-363.
23. Silva, C. *Flexy-Arm Remix*. 2015 [cited 2017 20-12]; Available from: https://www.thingiverse.com/thing:894705.

24. Wood, S. *Flexy-Hand*. 2014 [cited 2017 20-12]; Available from: https://www.thingiverse.com/thing:242639.
25. Wood, S. *Flexy-Hand 2*. 2014 [cited 2017 20-12]; Available from: https://www.thingiverse.com/thing:380665.
26. Wood, S. *Flexy-Hand - Filaflex Remix*. 2015 [cited 2017 20-12]; Available from: https://www.thingiverse.com/thing:754513.
27. Ultimaker, *Technical data sheet PLA*, Ultimaker, Editor. 2018.
28. Ultimaker, *Technical data sheet Tough PLA*, Ultimaker, Editor. 2018.
29. Ultimaker, *Technical data sheet TPU 95A*, Ultimaker, Editor. 2017.
30. Li, X., et al., *Impact behaviors of poly-lactic acid based biocomposite reinforced with unidirectional high-strength magnesium alloy wires.* Progress in Natural Science: Materials International, 2014. **24**(5): p. 472-478.
31. Qi, H.J. and M.C. Boyce, *Stress–strain behavior of thermoplastic polyurethanes.* Mechanics of Materials, 2005. **37**(8): p. 817-839.
32. Okubo, N., *Dynamic Viscoelastic Measurements of Thermoplastic Elastomer*. 1998, Hitachi High-Tech Science Corporation.
33. Patton, S., et al., *Characterization of Thermoplastic Polyurethane (TPU) and Ag-Carbon Black TPU Nanocomposite for Potential Application in Additive Manufacturing.* Polymers, 2017. **9**(1): p. 6.

Appendices

A. Technical drawings

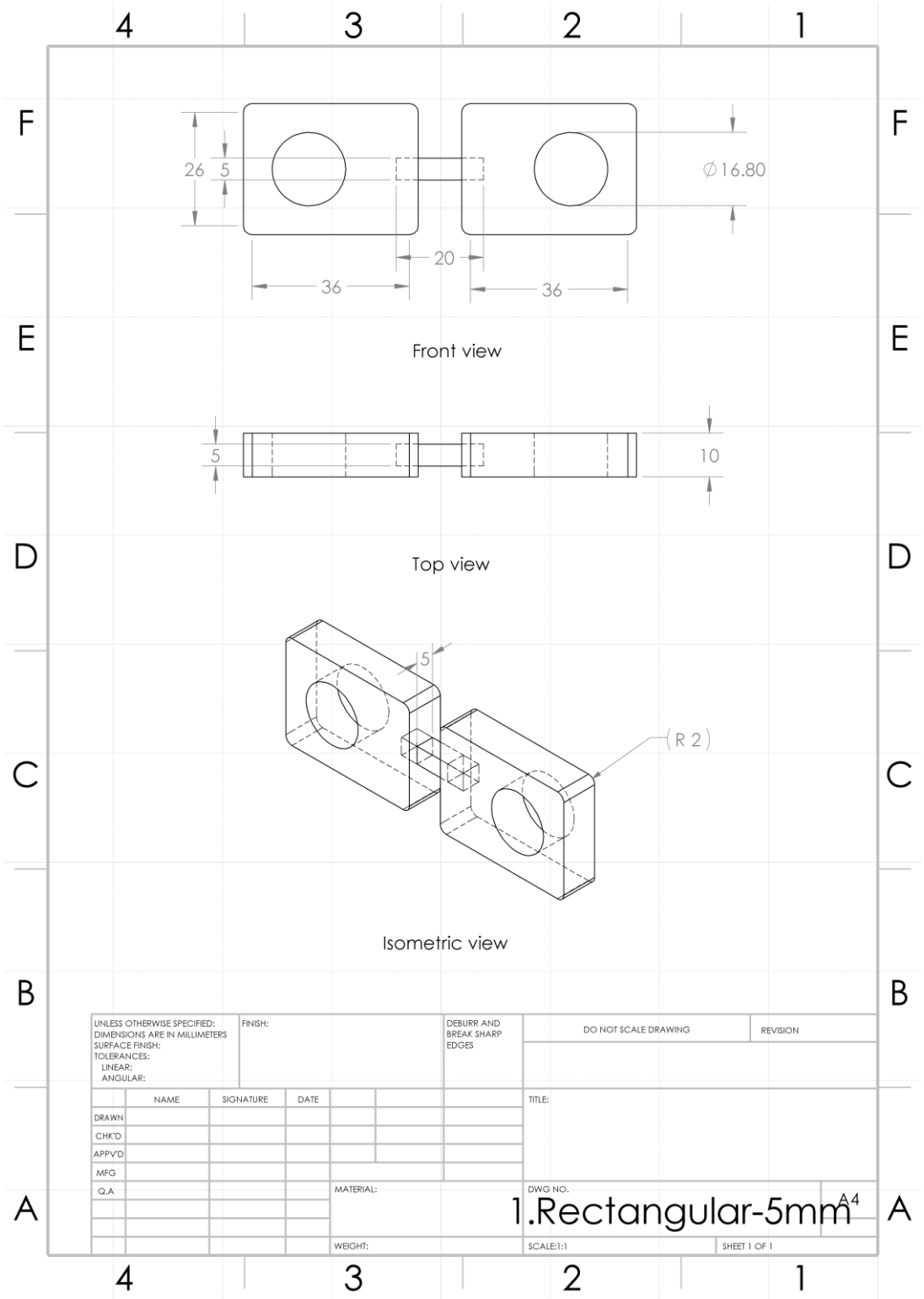

Figure A.1. The technical drawing of the bi-material compliant mechanism with rectangular-shaped interface in 5 mm thickness

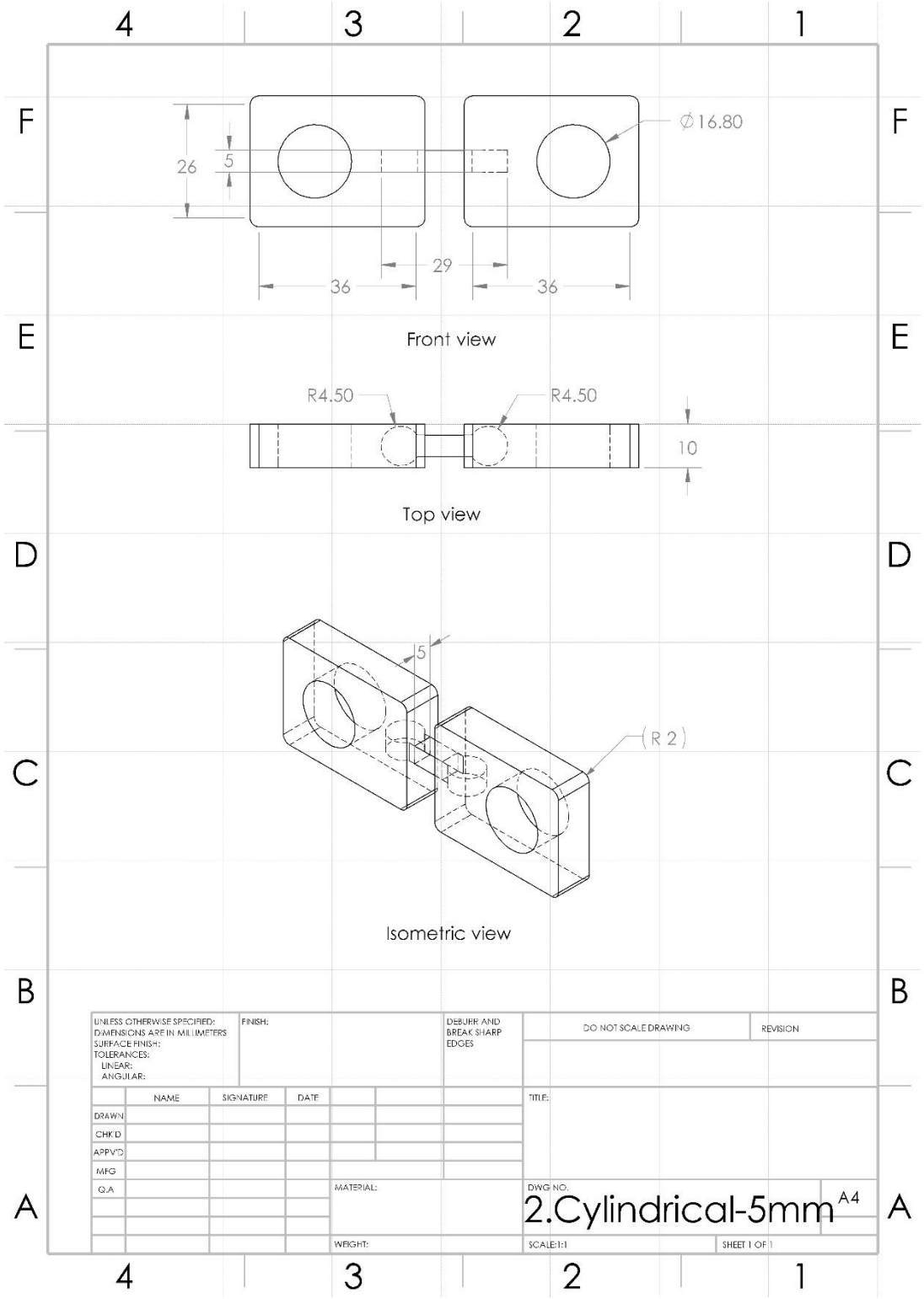

Figure A.2. The technical drawing of the bi-material compliant mechanism with cylindrical-shaped interface in 5 mm thickness

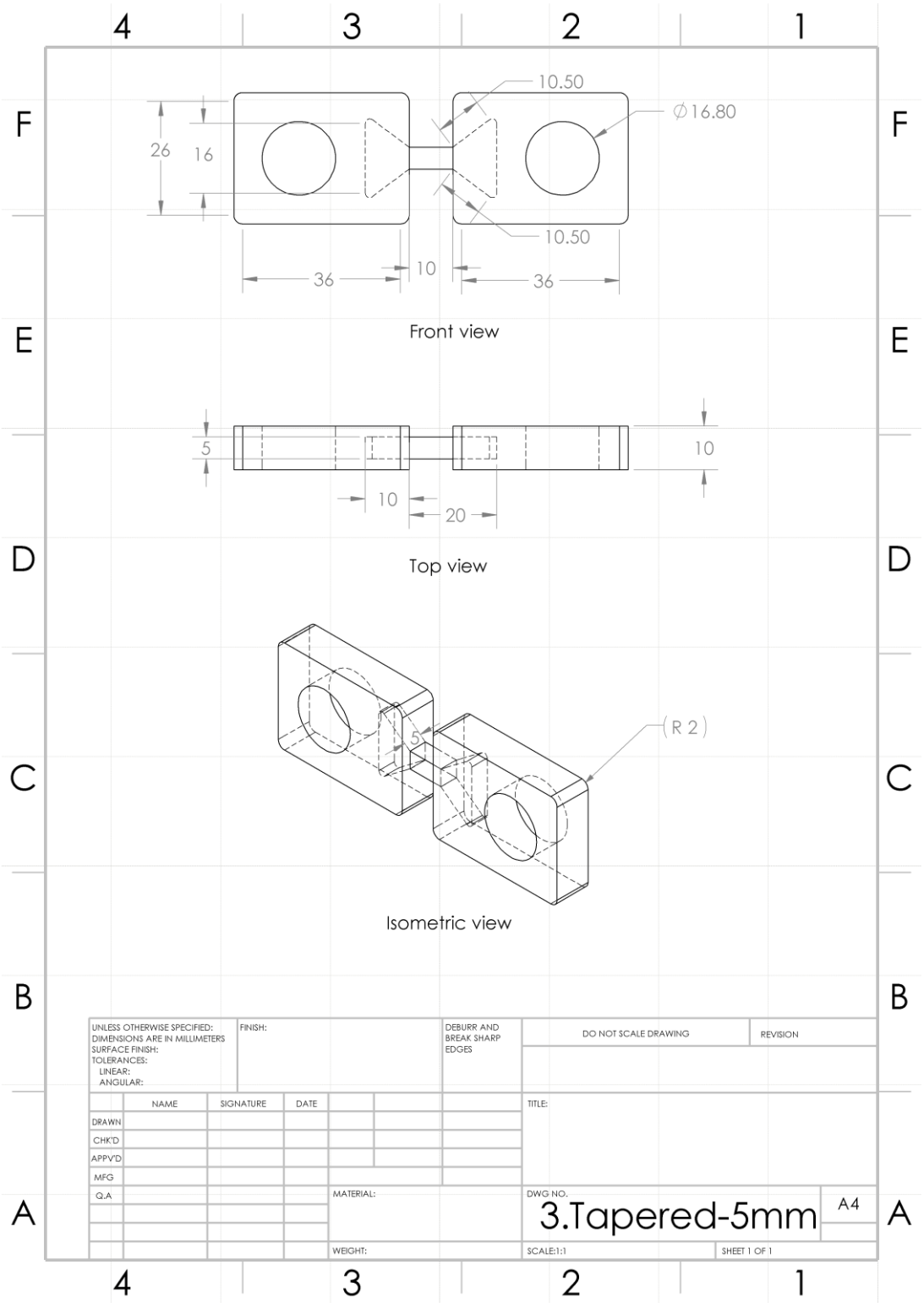

Figure A.3. The technical drawing of the bi-material compliant mechanism with tapered-shaped interface in 5 mm thickness

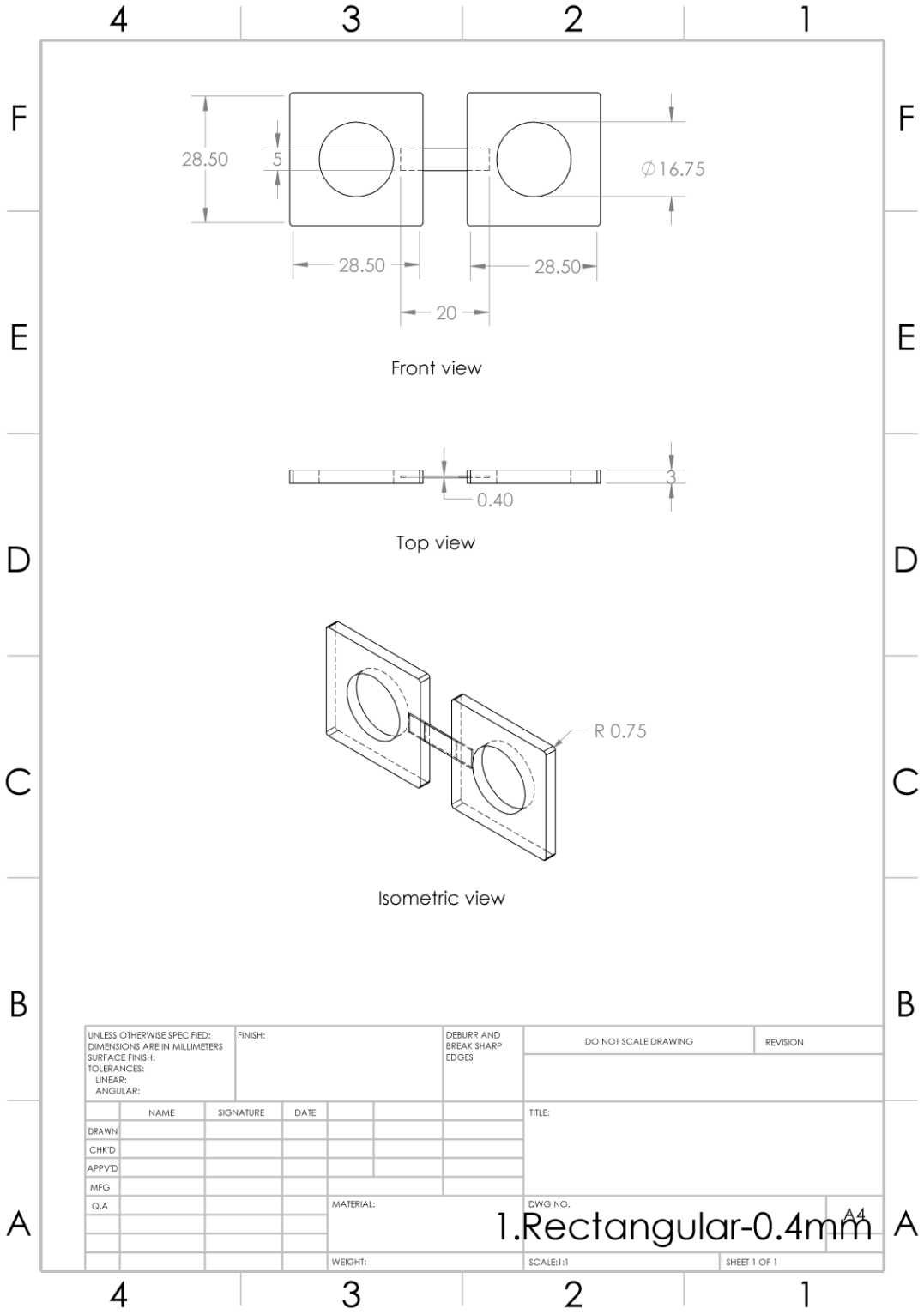

Figure A.4. The technical drawing of the bi-material compliant mechanism with rectangular-shaped interface in 0.4 mm thickness

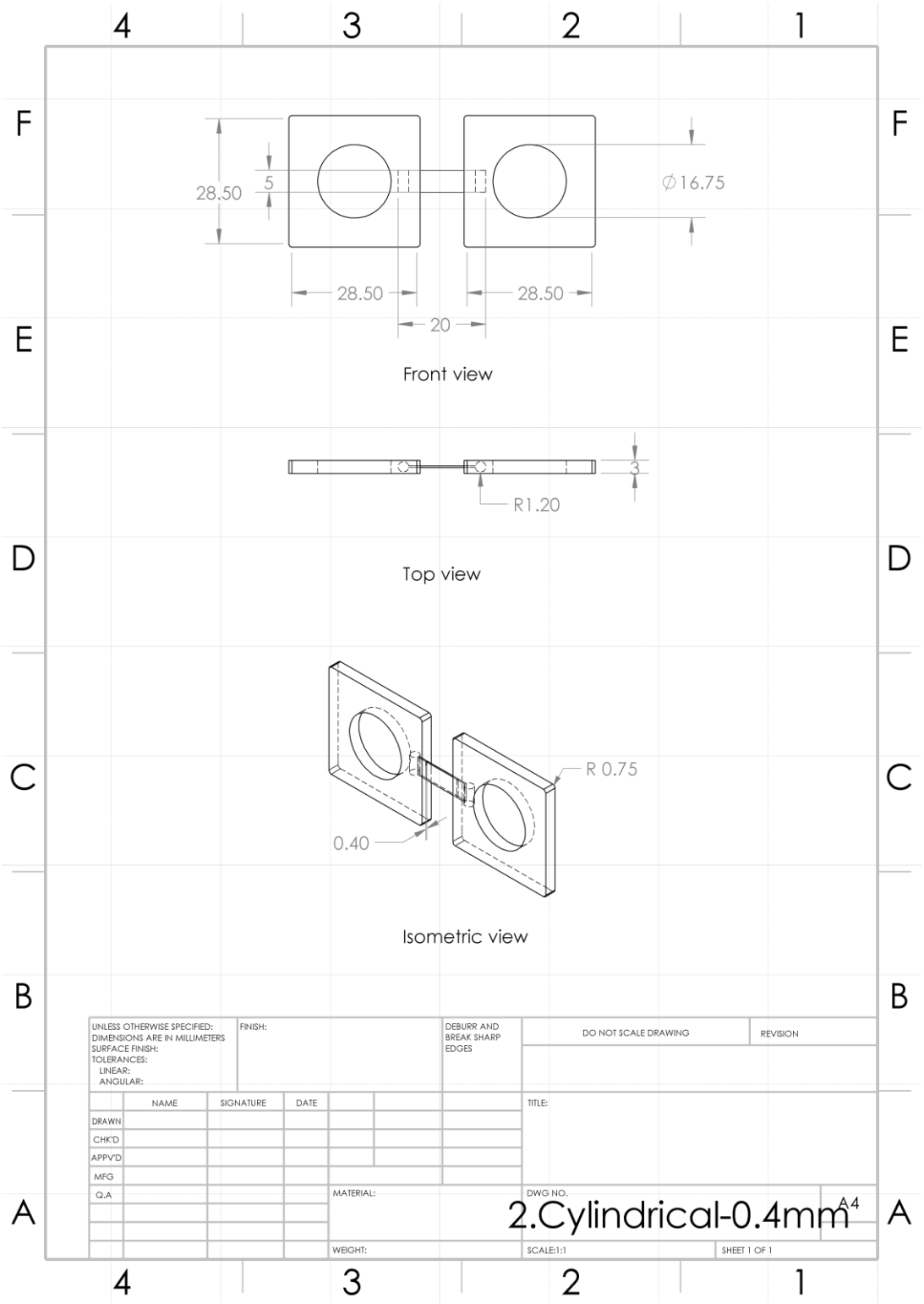

Figure A.5. The technical drawing of the bi-material compliant mechanism with cylindrical-shaped interface in 0.4 mm thickness

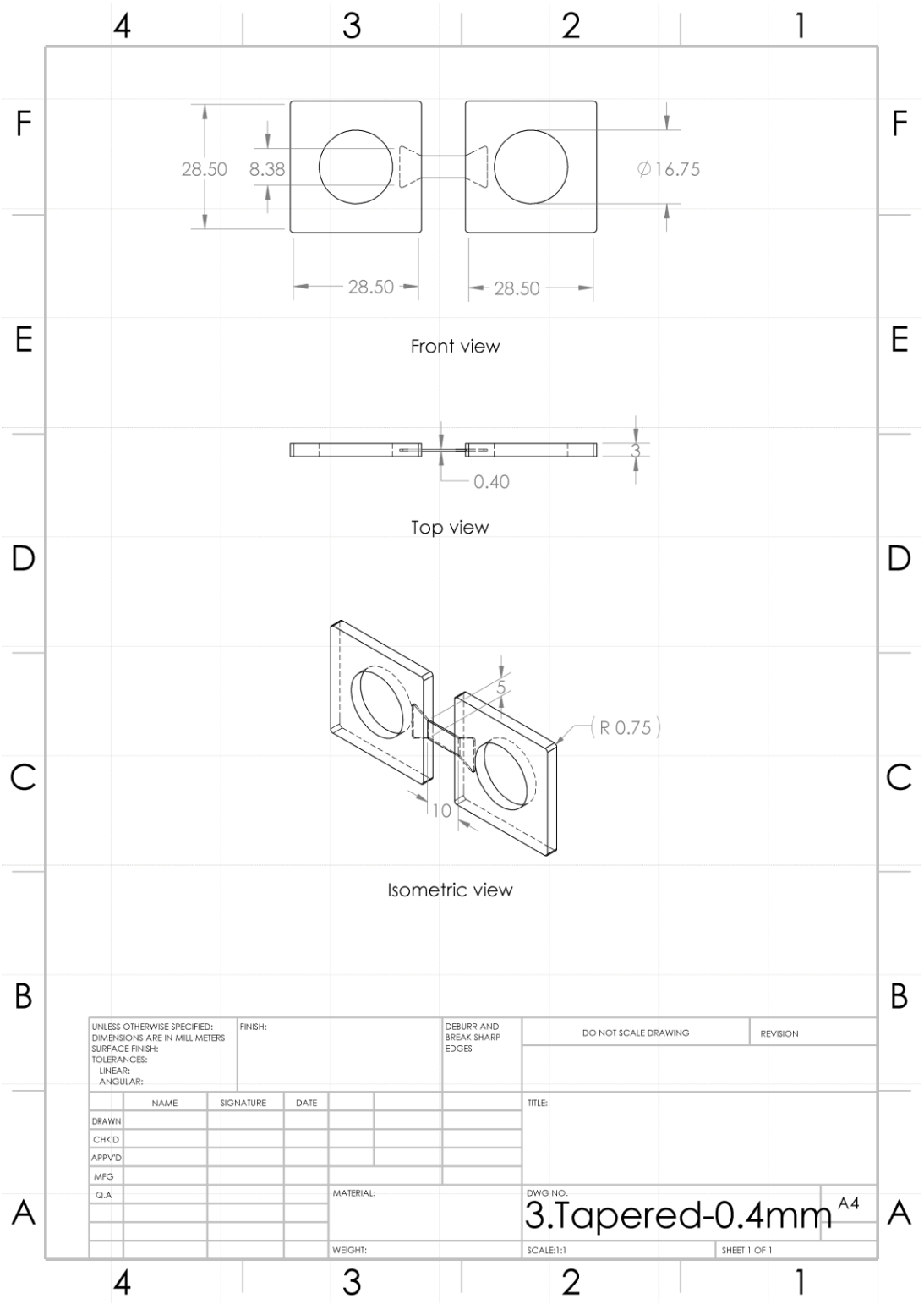

Figure A.6. The technical drawing of the bi-material compliant mechanism with tapered-shaped interface in 0.4 mm thickness

B. Printing Settings

All bi-material compliant mechanisms in this study were printed using Ultimaker 3 (ultimaker.com) with dual extrusion system where PLA/Tough PLA material was installed in extruder 1 and TPU 95A in extruder 2. Extruder 1 was set to the Cura default printing settings. However, several printing parameters in extruder 2 were modified. These settings are listed in **Table B**.

Table B. TPU 95A (extruder 2) printing settings that were modified from the Cura default printing settings

Parameter	Variable	Setting
Infill	Infill density	20%
	Gradual infill steps	0
Material	Enable retraction	Off
Speed	Printing speed	20 mm/s
	Travel speed	150 mm/s
	Initial layer speed	20 mm/s
Cooling	Enable print cooling	Off
	Minimum layer time	10 s
Support	Generate support	On
	Support extruder	Extruder 1
	Support placement	Everywhere
	Support density	15%
Build plate adhesion	Build plate adhesion type	Brim
	Build plate adhesion extruder	Extruder 1
	Brim width	5 mm

C. The comparison of stress distribution of geometries in Tough PLA-TPU 95A

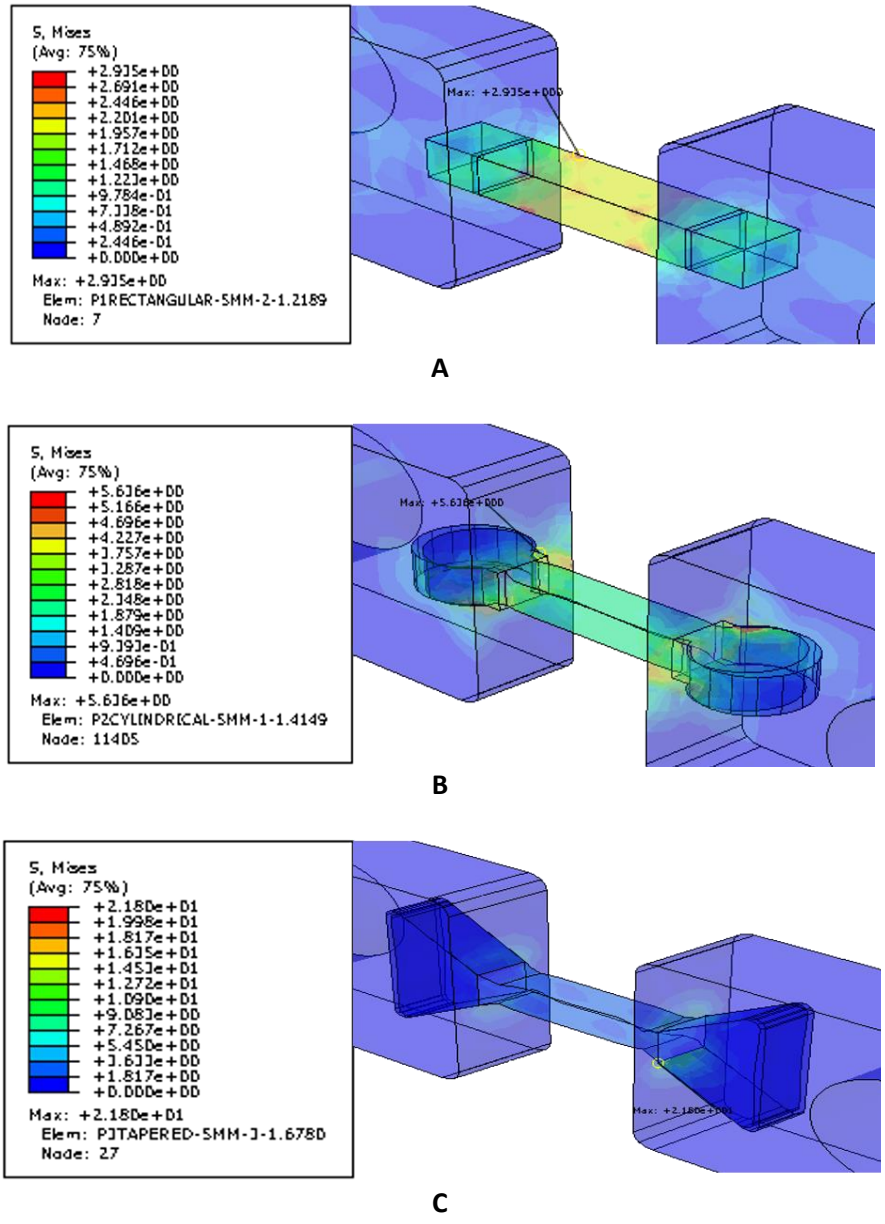

Figure C. Von Mises stress distribution of the Tough PLA-TPU95A mechanisms with A. rectangular, B. cylindrical, and C. tapered-shaped interface under axial loading of 50 N

D. The comparison of stress distribution of geometries in different materials

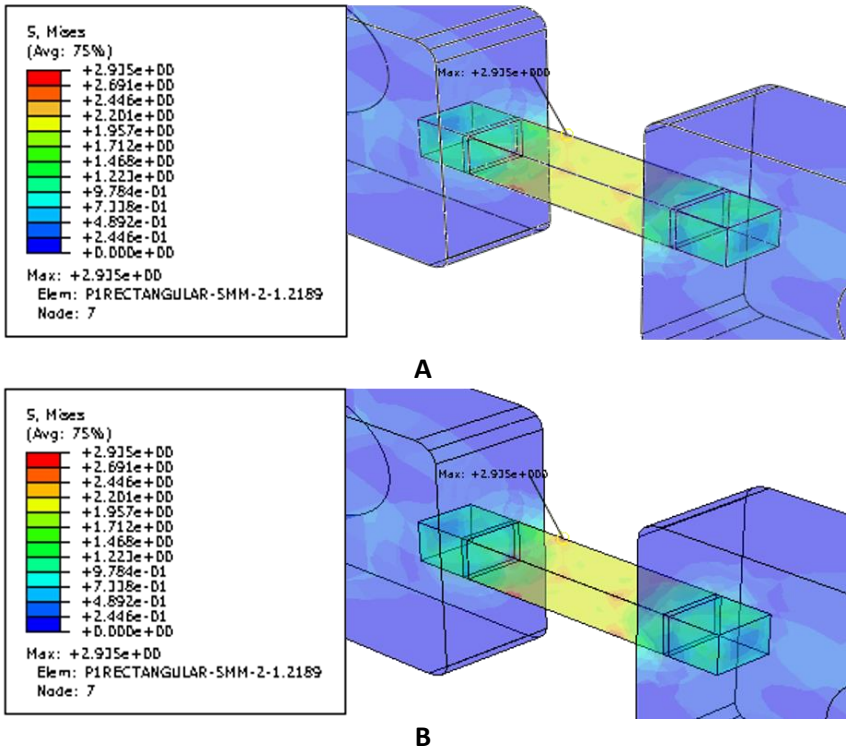

Figure D.1. Von Mises stress distribution of the mechanisms with rectangular interface under axial loading of 50 N. The model was simulated using different materials: A. PLA-TPU95A, and B. Tough PLA-TPU95A

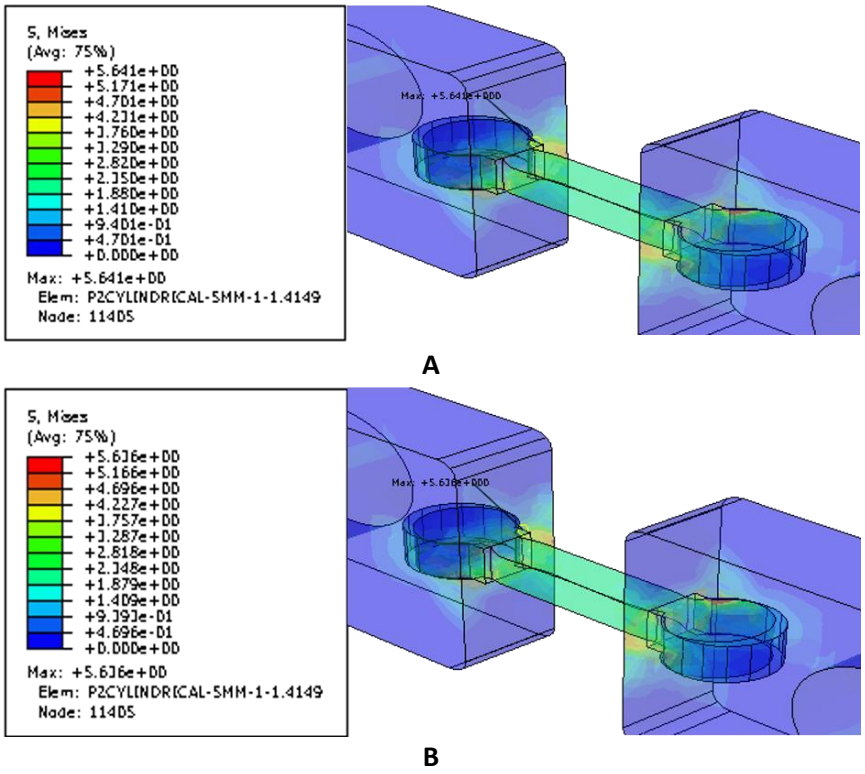

Figure D.2. Von Mises stress distribution of the mechanisms with cylindrical interface under axial loading of 50 N. The model was simulated using different materials: A. PLA-TPU95A, and B. Tough PLA-TPU95A

E. Fracture condition of the mechanisms, as simulated with Abaqus

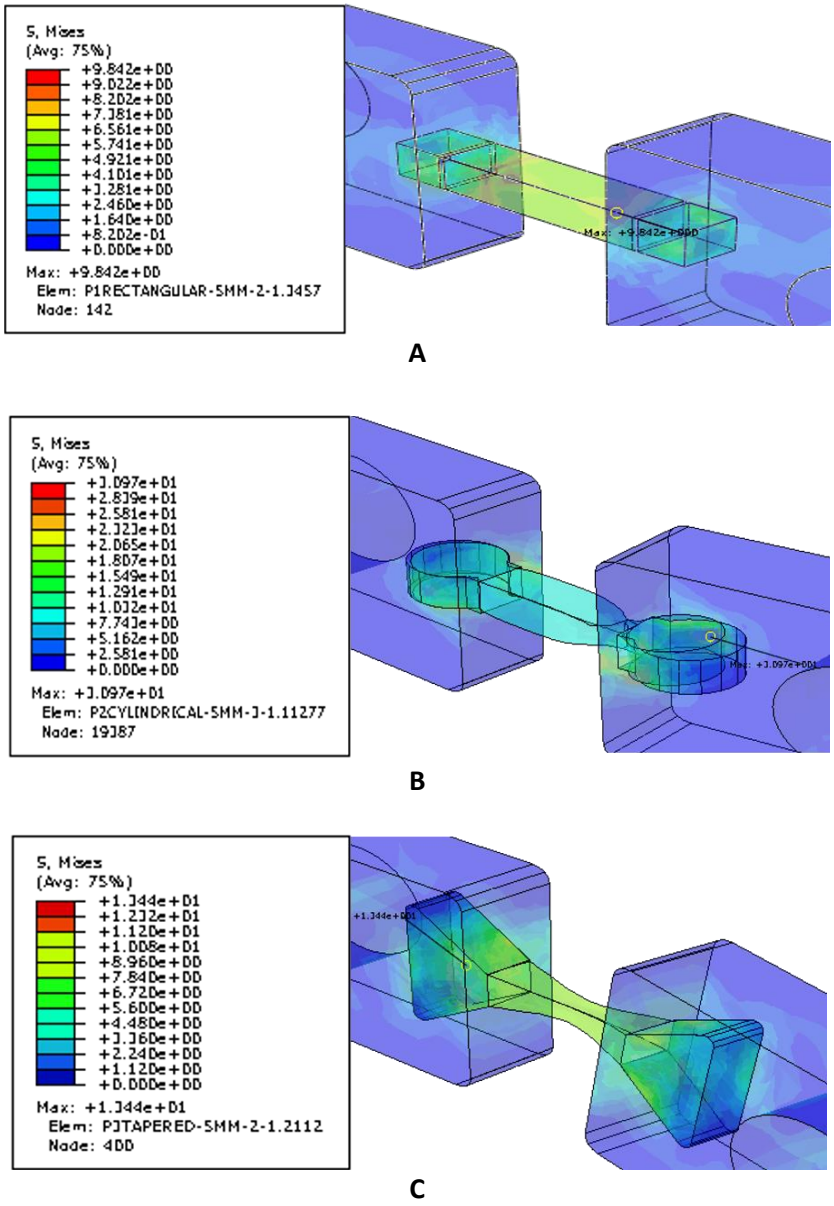

Figure E.1. Von Mises stress distribution of the PLA-TPU95A mechanisms with A. rectangular, B. cylindrical, and C. tapered-shaped interface when fracture occurred. The mechanisms were simulated using axial loading of 150 N, 198 N, and 218 N, respectively

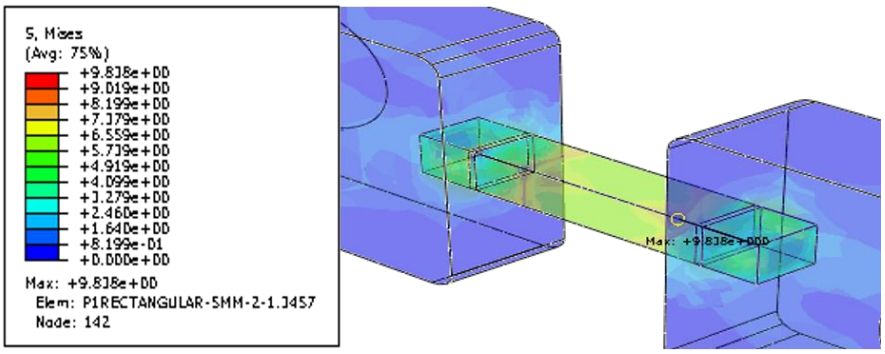

A

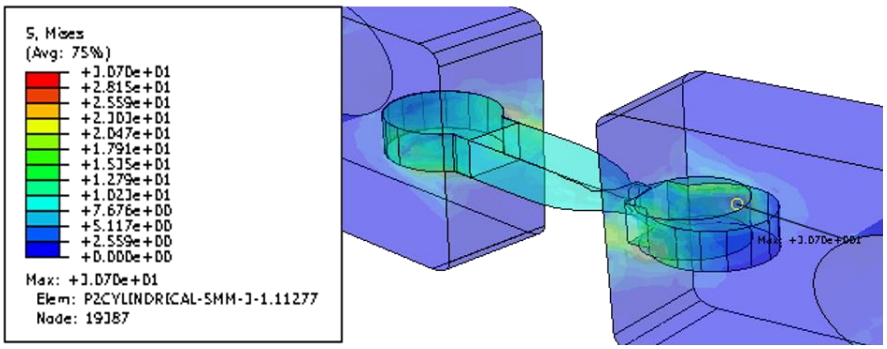

B

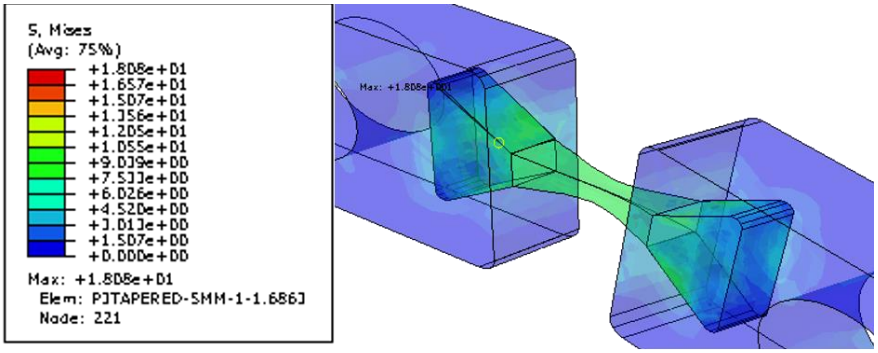

C

Figure E.2. Von Mises stress distribution of the Tough PLA-TPU95A mechanisms with A. rectangular, B. cylindrical, and C. tapered-shaped interface when fracture occurred. The mechanisms were simulated using axial loading of 150 N, 200 N and 220 N, respectively

F. Stress and strain data from finite element simulation

This section consists of stress and strain data of each model under various loading conditions. The values of maximum load in experimental fatigue testing of rectangular interface as well as the values of load when other mechanisms reached 0.55 strain during tensile testing are printed in bold.

Table F.1. Von Mises stress and strain data of a model with PLA-TPU95A rectangular interface

Load (N)	S (MPa)	E (mm/mm)
25	1.45	0.1431
32	**1.86**	**0.1861**
50	2.93	0.2963
75	4.89	0.4844
100	7.48	0.7336

Table F.2. Von Mises stress and strain data of a model with Tough PLA-TPU95A rectangular interface

Load (N)	S (MPa)	E (mm/mm)
25	1.45	0.1431
39	**2.28**	**0.2292**
50	2.93	0.2963
75	4.90	0.4854
100	7.50	0.7348

Table F.3. Von Mises stress and strain data of a model with PLA-TPU95A cylindrical interface

Load (N)	S (MPa)	E (mm/mm)
50	5.64	0.5159
75	8.61	0.7817
91	**10.58**	**0.966**
100	11.69	1.117
125	14.99	1.67
150	15.81	1.904

Table F.4. Von Mises stress and strain data of a model with Tough PLA-TPU95A cylindrical interface

Load (N)	S (MPa)	E (mm/mm)
50	5.61	0.5173
75	8.61	0.784
100	11.69	1.124
102	**11.94**	**1.169**
125	14.99	1.679
150	18.29	2.656

Table F.5. Von Mises stress and strain data of a model with PLA-TPU95A tapered-shaped interface

Load (N)	S (MPa)	E (mm/mm)
50	21.80	0.396
75	34.36	0.602
100	46.53	0.8081
110	**51.41**	**0.8906**
125	58.10	1.032
150	62.16	1.445

Table F.6. Von Mises stress and strain data of a model with Tough PLA-TPU95A tapered-shaped interface

Load (N)	S (MPa)	E (mm/mm)
50	22.04	0.1964
75	34.73	0.6027
100	47.05	0.8091
110	**51.97**	**0.8917**
125	58.68	1.035
150	66.86	1.455